Review Article

JCBFM

Journal of Cerebral Blood Flow & Metabolism
2022, Vol. 42(6) 911–934

DOI: 10.1177/0271678X221076570
journals.sagepub.com/home/jcbfm
SAGE

Human brain functional MRS reveals interplay of metabolites implicated in neurotransmission and neuroenergetics

Yury Koush[1], Douglas L Rothman[1,2], Kevin L Behar[1,3], Robin A de Graaf[1,2] and Fahmeed Hyder[1,2]

Abstract

While functional MRI (fMRI) localizes brain activation and deactivation, functional MRS (fMRS) provides insights into the underlying metabolic conditions. There is much interest in measuring task-induced and resting levels of metabolites implicated in neuroenergetics (e.g., lactate, glucose, or β-hydroxybutyrate (BHB)) and neurotransmission (e.g., γ-aminobutyric acid (GABA) or pooled glutamate and glutamine (Glx)). Ultra-high magnetic field (e.g., 7T) has boosted the fMRS quantification precision, reliability, and stability of spectroscopic observations using short echo-time (TE) ^{1}H-MRS techniques. While short TE ^{1}H-MRS lacks sensitivity and specificity for fMRS at lower magnetic fields (e.g., 3T or 4T), most of these metabolites can also be detected by J-difference editing (JDE) ^{1}H-MRS with longer TE to filter overlapping resonances. The ^{1}H-MRS studies show that JDE can detect GABA, Glx, lactate, and BHB at 3T, 4T and 7T. Most recently, it has also been demonstrated that JDE ^{1}H-MRS is capable of reliable detection of metabolic changes in different brain areas at various magnetic fields. Combining fMRS measurements with fMRI is important for understanding normal brain function, but also clinically relevant for mechanisms and/or biomarkers of neurological and neuropsychiatric disorders. We provide an up-to-date overview of fMRS research in the last three decades, both in terms of applications and technological advances. Overall the emerging fMRS techniques can be expected to contribute substantially to our understanding of metabolism for brain function and dysfunction.

Keywords

Neuroimaging, functional MRS, neuroenergetics, neurotransmission, J-difference editing (JDE), γ-aminobutyric acid (GABA), glutamate, Glx (glutamate and glutamine), lactate, β-hydroxybutyrate (BHB)

Received 1 August 2021; Revised 26 December 2021; Accepted 5 January 2022

Introduction

A wide range of magnetic resonance imaging (MRI) and spectroscopy (MRS) methods are routinely applied in explorations of the human brain, spanning from basic sciences to clinical research.[1,2] The most popular is functional MRI (fMRI), which is widely used in creating biomarkers of neurological and neuropsychiatric disorders. The fMRI method is based on blood oxygen level-dependent (BOLD) contrast to indirectly localize brain function associated with task-induced activations (BOLD signal increase) or deactivations (BOLD signal decrease), as well as intrinsic resting-state brain activity from the spontaneous BOLD signal fluctuations.[3,4] BOLD contrast reflects changes in the local magnetic field gradients caused by paramagnetic deoxyhemoglobin packed inside red blood cells, which in turn affects transverse relaxation time of tissue water protons (T_2 or T_2*). Changes in BOLD signal are associated with complex interactions between hemodynamic and

[1]Magnetic Resonance Research Center, Department of Radiology & Biomedical Imaging, Yale University, New Haven, CT, USA
[2]Department of Biomedical Engineering, Yale University, New Haven, CT, USA
[3]Department of Psychiatry, Yale University, New Haven, CT, USA

Corresponding authors:
Yury Koush, Magnetic Resonance Research Center, Yale University, 300 Cedar Street, New Haven, CT 06519, USA.
Email: yury.koush@yale.edu

Fahmeed Hyder, Yale University 300 Cedar St New Haven, CT Connecticut 06510, USA.
Email: fahmeed.hyder@yale.edu

metabolic variations.[1,5] Although progress has been achieved for the interpretation of BOLD contrast in terms of the cerebral blood flow (CBF), cerebral blood volume (CBV), and the cerebral metabolic rates of glucose (CMR_{Glc}) and oxygen (CMR_{O2}) consumption,[1,2,6,7] the underlying neurometabolic modulations are still being explored.[1,2]

Technological advances in ^{1}H-MRS in vivo have improved rapidly, leading to a substantial increase in spectral quality allowing robust quantification of low concentration metabolites in human brain.[8,9] As a result, much interest has emerged in the measurement of metabolite levels implicated in neuroenergetics and neurotransmission mediating physiological activity during task and rest conditions, which initiated an emergence of functional ^{1}H-MRS (fMRS). For instance, fMRS measurements of task-associated changes in glucose, lactate or β-hydroxybutyrate (BHB) can provide insights into overall brain energetics, while measurements of changes in glutamate (or pooled glutamate and glutamine termed Glx) and γ-aminobutyric acid (GABA) can provide insights into excitatory and inhibitory neuromodulation. Under normal conditions, glucose is the primary brain energy substrate and BHB is an additional energy substrate during starvation, whereas lactate is a byproduct of glycolysis and Glx and GABA are associated with major excitatory and inhibitory actions in the neuropil. Typically, fMRS addresses hypotheses pertaining to changes in neurometabolic alterations characteristic of physiological stimuli and rest conditions. Specifically, stimuli-induced changes in glutamate/glutamine/GABA are hypothesized to reflect changes in functional excitation-inhibition balance, and changes in glucose/lactate/BHB are hypothesized to reflect changes in functional energetics. Changes in other metabolites detected by ^{1}H-MRS (e.g., myo-inositol, glutathione, aspartate) are less frequently observed in fMRS studies and thus require further reproducibility tests prior to specific hypotheses testing.

Positron emission tomography (PET) allows quantification of glucose metabolism[10] related to glucose transport and phosphorylation (CMR_{Glc}) using ^{18}F-fluorodeoxyglucose (FDG). Recently, FDG-PET has been shown to be feasible for dynamic measure of spontaneous fluctuations of CMR_{Glc} at rest and in response to physiological stimuli ($\sim$minutes timescale).[11] Furthermore, PET using different methods can measure resting or task-induced changes in CBF and CMR_{Glc},[10] similar to what MRI/MRS methods can provide.[1] Although single-photon emission computed tomography (SPECT) can be used to image CBF, it is less preferred compared to MRI and/or PET in functional studies. Currently, there are no PET and SPECT methods that can measure levels of metabolites like glutamate, GABA, Glx, lactate, BHB in human brain. There are, however, PET ligands for glycine transporters (GlyT1)[12,13] and glutamate receptors (mGluR5)[14,15] that can indirectly reflect intrasynaptic glycine and glutamate levels, whereas MRS measures of metabolites predominantly reflect intracellular levels. PET also allows steady-state estimates of GABA and serotonin[16,17] receptors and dopamine transporter.[18] Thus, despite low sensitivity of functional ^{1}H-MRS, it is the only non-invasive technique available for simultaneous quantitative measurement of multiple neurochemicals in vivo, with as many as six metabolites showing stimulus-related changes out of twenty metabolites quantified at 7.0T. When combined with isotopic enrichment of appropriate substrates, ^{1}H-MRS with indirect ^{13}C detection, as well as other MR-sensitive nuclei (e.g., ^{13}C, ^{17}O, ^{19}F) can be used to measure fluxes through metabolic pathways related to neurotransmission and neuroenergetics (for review, see[1]) Particularly, ^{13}C-MRS, ^{17}O-MRS and ^{1}H-MRS provide rates of CMR_{O2}, ^{13}C-MRS, ^{1}H-MRS and ^{19}F-MRS provide rates of CMR_{Glc}, as well as ^{31}P-MRS provides rates of ATP synthesis in mitochondria. ^{13}C-MRS has been also used to study functional changes in neuronal tricarboxylic acid (TCA) cycle turnover during visual stimulation.[19] This review presents an overview of methodological advances in functional MRS (fMRS), and fMRS studies investigating consistent metabolic changes implicated in neuroenergetics and neurotransmission underlying brain function in healthy controls, which supplements previous reviews focused on the interpretation of observed metabolic changes,[20] specifically glutamate changes,[21–23] and multimodal imaging.[1,24]

Initial functional ^{1}H-MRS findings of task-induced changes in neuroenergetics

Brain energy from glucose oxidation ($CMR_{Glc(ox)}$) is critical for rest and stimulated conditions.[25] Regional CBF, CMR_{Glc} and CMR_{O2} values measured by PET are tightly coupled throughout the resting human brain,[10] where the ratio of CMR_{O2} to CMR_{Glc} provides the oxygen-to-glucose index (OGI) and the ratio of CMR_{O2} to CBF leads to the oxygen extraction fraction (OEF). The OGI indicates the degree of $CMR_{Glc(ox)}$ in a given region. Since the normal brain is well oxygenated, the degree of deviation of the OGI from the theoretical maximum of 6 is often termed aerobic glycolysis.[26] The OEF indicates the degree of oxygen transported to the tissue in relation to the oxygen remaining in the blood, and its role in interpretation of BOLD signal is critical.[6] Recent studies suggest that

for the resting human brain there exist very small regional differences in OGI and OEF.[10,26] During physiological stimulation there is modest uncoupling between CMR_{O2} and CMR_{Glc}, as well as between CMR_{O2} and CBF in localized brain areas. PET and MRS studies have contributed much to our current knowledge about OGI and OEF changes during brain activation and deactivation (for historical perspective, see[2]).

Steady-state stimuli-induced activation triggers regional uncoupling between CBF and CMR_{O2} (where $\Delta CBF\% > \Delta CMR_{O2}\%$ implies reduced OEF), which is consistent with the increased BOLD effect during stimulation compared to baseline.[27,28] Similarly, steady-state stimuli-induced activation also shows regional uncoupling between CMR_{Glc} and CMR_{O2} (where $\Delta CMR_{Glc}\% > \Delta CMR_{O2}\%$ implies OGI drop), which suggests less efficient $CMR_{Glc(ox)}$ and some lactate increase during task.[29–31] These types of flow-metabolism uncouplings specifically occur over longer time scales after stimulation onset, as typically measured by fMRS studies. While the task-induced increase of lactate suggests a rise in aerobic glycolysis and flux from pyruvate to lactate, its subsequent fate in the neuropil is less clear. For example, lactate could serve as a signaling molecule between neurons and glial cells,[2,32] but lactate could also serve as an alternative energy substrate.[2,33,34] Recently, the role of lactate was further extended by suggesting that it could act as a blood volume transmitter of cellular signals (vasodilation) that also regulates energy metabolism in large neuronal ensembles.[28,35] Much less is known about lactate changes associated with stimuli-induced deactivation. These different fates for lactate are better discussed in each of the references mentioned above.

^{1}H-MRS in human brain provides insights into the underlying metabolic and physiologic modulations from rest. Since task-induced increase in CMR_{Glc} may be associated with a rise in lactate and fall in glucose,[2,22,31,34,36,37] these changes can serve as the basis for fMRS measurements. Consistently, early fMRS studies detected lactate increase[31,38,39] and glucose decrease[37,39,40] in visual cortex (VC) during visual stimulation (Table 1). In addition to studying VC activation, lactate elevations were associated with basal ganglia activation during finger tapping,[41] and with inferior frontal gyrus activation during silent word generation task.[42,43] Of note, single voxel (or single volume) spatial localization is mostly used for (f) MRS acquisitions, with typical voxel size of 8 mL or larger. The size of the single (f)MRS voxel is typically a compromise between the desired spatial specificity and signal-to-noise ratio (SNR) of the target low-concentrated molecules given magnetic field strength and MRS method. Relatively large single (f)MRS voxels allow for increased spectral SNR, optimization of field inhomogeneity, and efficient water and lipid suppression, but these come at the cost of limited spatial sampling, and thus these signals cannot be analyzed like dynamic fMRI data.

The initial fMRS study was performed by Prichard and coworkers[31] at 2.1T on 5 subjects using a long echo-time (TE) localized spin-echo sequence and surface transmit/receive radio frequency (RF) coil. At this long TE, macromolecules were largely suppressed, as shown by the lactate doublet in the spectra. The mean lactate concentration was measured at 0.71 mM, similar to earlier report from the same group using lactate editing of 0.60 mM.[44] An average lactate increase of 54% was observed with a range from 30–90%, which reached a maximum by 3 minutes and slightly declined at 9 minutes (time resolution of measurements was 6 minutes). Although the percent increase in lactate was higher than most recent reports, the average lactate increment (when renormalized to creatine at 8.0 mM) was 0.29 mM which is within the range of lactate concentration increments reported in more recent studies at ultrahigh field.[45–50] Prior to 2005 (Table 1) all fMRS studies were performed at what is considered today relatively low field (1.5T to 2.1T). The use of long TE suppresses short T_2 lipid and macromolecule signals, but the long TE lowers spectral SNR. However, several studies implemented short TE for fMRS using the stimulated echo acquisition mode (STEAM)[8] pulse sequence at 2.0T.[39,40] Several early studies at these lower magnetic field failed to show any task-induced alterations and failed to quantify basal level metabolites most likely due to the reduced specificity from long TE, use of volume transmit/receive coils, and insufficient duration of stimulation epochs (for examples of studies without reported metabolic changes, see reviews[20,51]). For studies with sufficient SNR to detect lactate, the majority of studies reported a higher percent increase than most studies after 2005 that used higher magnetic fields (Table 1). A partial explanation is that lactate in the early studies using a long TE was not impacted by macromolecules, resulting in a higher percentage change for the same absolute increment in lactate concentration. Another explanation is large reported intrasubject variation in both the earlier low field and recent high field fMRS studies. As described below, much of this variation is likely biological as it correlates with the increase in the magnitude of the BOLD activation. In the pre-2005 studies, many of which used small subject numbers, this factor alone could have led to a 2-fold or more variation in the mean percentage increments (and may still explain much of the variation in recent studies when differences in stimulation paradigm, region, and partial activation

Table 1. Combined fMRI and fMRS for various brain regions shows task-induced changes in various metabolites.

area	task	Bo (T) Vendor	fMRI	fMRS sequence (TE, ms)	Δmetabolite	reference
VC	visual stimulation	2.1Bruker	activation*	SE MRS (100)	54%↑Lac	Prichard et al. 1991[31]
VC	visual stimulation	2 Gyroscan	activation*	SE MRS (272)	250%↑Lac	Sappey-M. et al. 1992[38]
VC	visual stimulation	2 Siemens	activation*	STEAM (20)	50%↓Glc	Merboldt et al. 1992[40]
VC	visual stimulation	2.1 Bruker	activation*	SE MRS (48)	31%↓Glc	Chen et al. 1993[37]
left BG	motor tapping	1.5 Siemens	activation*	SE MRS (270)	20%↑Lac	Kuwabara et al. 1995[41]
VC	visual stimulation	2 Siemens	activation	STEAM (20)	68%↑Lac, 40%↓Glc	Frahm et al. 1996[39]
left IFG	word generation	1.5 GE	activation	PRESS (288)	54%↑Lac	Urrila et al. 2003[42]
left IFG	word generation	1.5 GE	activation	PRESS (288)	40%↑Lac	Urrila et al. 2004[43]
rACC	foot cold pain	4 Varian	activation*	STEAM (20)	9%↑Glu	Mullins et al. 2005[161]
left M1	motor squeezing	3 Varian	activation*	MEGA PRESS (68)	20%↓GABA	Floyer-Lea et al. 2006[97]
VC	visual stimulation	1.5 GE	activation*	PRESS (288)	7%↑Lac	Maddock et al. 2006[162]
VC	visual stimulation	7 Varian	activation	STEAM (6)	23%↑Lac, 3%↑Glu, 15%↓Asp	Mangia et al. 2007a[45]
VC	visual stimulation	7 Varian	activation	STEAM (6)	18%↑Lac	Mangia et al. 2007b[46]
rACC	leg heat pain	3 Siemens	activation*	PRESS (20)	15%↑GABA	Kupers et al. 2009[86]
mPFC	threat of shock	3 GE	activation*	JDE PRESS (68)	18%↓GABA	Hasler et al. 2010[98]
VC	visual stimulation	3 Siemens	activation	PRESS (30)	50%↑Lac	Lin et al. 2010[30]
left aIC	forearm heat pain	3 Siemens	activation*	PRESS (30)	18%↑Glu	Gussew et al. 2010[81]
VC	physical exercise	1.5 GE	na	JDE PRESS (144)	18%↑Glx, 19%↑Lac	Maddock et al. 2011[114]
left IC	dental electrical pain	3 Philips	activation*	PRESS (30)	16%↑Glx, 55%↑Glu, 10%↓mI	Gutzeit et al. 2011[82]
VC	visual stimulation	7 Philips	activation	STEAM (15)	3%↑Glu, 9%↑Lac, 8%↑GSH, 10%↓Asp, 12%↓Gly, 6%↓Gln	Lin et al. 2012[72]
left dlPFC	working memory	3 GE	activation	MEGA PRESS (68)	4%↑GABA	Michels et al. 2012[101]
VC	visual stimulation	7 Siemens	activation	SPECIAL (6)	4%↑Glu, 19%↑Lac, 12%↓Glc	Schaller et al. 2013[47]
left aIC	dental electrical pain	3 Philips	activation*	PRESS (30)	15%↑Glx, 6%↑Glu, 32%↑Gln, 7%↓mI	Gutzeit et al. 2013[83]
right aIC	dental electrical pain	3 Philips	activation*	PRESS (30)	14%↑Glx, 6%↑Glu, 28%↑Gln, 13%↓mI	Gutzeit et al. 2013[83]
left pIC	dental electrical pain	3 Philips	activation*	PRESS (30)	14%↑Glx, 7%↑Glu, 28%↑Gln	Gutzeit et al. 2013[83]
right pIC	dental electrical pain	3 Philips	activation*	PRESS (30)	13%↑Glx, 8%↑Glu, 20%↑Gln, 6%↓mI	Gutzeit et al. 2013[83]
left MC	motor tapping	7 Siemens	activation	SPECIAL (12)	2%↑Glu, 17%↑Lac	Schaller et al. 2014[48]
LOC	visual repetition priming	3 Philips	activation*	PRESS (40)	12%↑Glu	Lally et al. 2014[79]
VC	visual stimulation	7 Siemens	activation	sLASER (26)	3%↑Glu, 30%↑Lac, 5%↓Asp, 16%↓Glc	Bednarik et al. 2015[49]
dACC	forearm heat pain	3 Siemens	activation*	MEGA PRESS (68)	22%↑Glx, 15%↓GABA	Cleve et al. 2015[94]
VC	forearm heat pain	3 Siemens	activation*	MEGA PRESS (68)	16%↑Glx, 13%↓GABA	Cleve et al. 2015[94]
left LOC	visual stimulation	3 Philips	activation	fMRI-fMRS: PRESS WS-PRESS (105)	12%↑Glu	Apsvalka et al., 2015[84]
dACC	Stroop task	7 Siemens	activation*	STEAM (10)	3%↑Glu	Taylor et al. 2015b[76]

(continued)

Table 1. Continued.

area	task	Bo (T) Vendor	fMRI	fMRS sequence (TE, ms)	Δmetabolite	reference
dACC	Stroop task	7 Siemens	activation	STEAM (10)	2%↑Glu (healthy)	Taylor et al. 2015a[75]
rACC	mental imagery	3 Philips	deactivation	PRESS (24)	2%↑Glx	Huang et al. 2015[115]
VC	physical exercise	3 Siemens	na	MEGA PRESS (68)	3%↑Glu, 7%↑GABA	Maddock et al. 2016[113]
VC	physical exercise	3 Siemens	na	PRESS (144)	5%↑Glu	Maddock et al. 2016[113]
rdACC	physical exercise	3 Siemens	na	PRESS (144)	5%↑Glu	Maddock et al. 2016[113]
VC	physical exercise	3 Siemens	na	PRESS (144)	6%↑Glu	Maddock et al. 2016[113]
VC	physical exercise	3 Siemens	na	PRESS (30)	7%↑Glu	Maddock et al. 2016[113]
ACC	Stroop task	3 Siemens	activation	SPECIAL (9)	4%↑Glu, 7%↑Gln, 22%↓GABA	Kuhn et al. 2016[77]
right VC	visual stimulation	7 Siemens	activation	SPECIAL (6)	7%↑Lac, 5%↓GABA	Mekle et al. 2017[73]
left MC	motor clenching	7 Philips	activation	MEGA sLASER (72)	11%↑Glx, 12%↓GABA	Chen et al. 2017[92]
right Hipp	associative learning	3 Siemens	activation*	PRESS (23)	4–11%↑Glu	Stanley et al. 2017[80]
dACC	forearm heat pain	3 Siemens	activation*	STEAM (6.5)	2%↓Glu	Chiappelli et al. 2017[87]
VC	visual stimulation	7 Siemens	activation	fMRI-fMRS: GE EPI-sLASER (36)	2%↑Glu	Ip et al. 2017[56]
VC	visual stimulation	7 Siemens	activation	sLASER (26)	3%↑Glu, 29%↑Lac, 5%↓Asp	Bednarik et al. 2018[71]
VC	visual stimulation	3 Siemens	activation	MEGA PRESS (68)	10%↑Glx, 20%↓GABA	Kurcius et al. 2018[93]
left dlPFC	working memory	3 Siemens	activation*	PRESS (23)	3%↑Glu	Woodcock et al. 2018[85]
VC	visual stimulation	7 Siemens	activation	sLASER (40)	5%↑Glu	Martinez-M. et al. 2019[105]
VC	visual stimulation	7 Siemens	deactivation	sLASER (40)	8%↓Glc, 4%↓Glu, 4%↑GSH	Martinez-M. et al. 2019[105]
right MC	motor tapping	4 Bruker	activation	MEGA sLASER (144)	9%↑Lac	Koush et al. 2019[53]
left MC	motor learning	7 Siemens	activation*	sLASER (36)	20%↓GABA	Kolasinski et al. 2019[78]
VC	visual stimulation	7 Siemens	activation	fMRI-fMRS: GE EPI-sLASER (36)	1.5%↑Glu	Ip et al. 2019[55]
dACC	reinforcement learning	3 Siemens	activation*	MEGA PRESS (68)	3–10%↑GABA	Bezalel et al. 2019[112]
VC	visual stimulation	7 Siemens	activation	SPECIAL (16)	2%↑Glu, 21%↑Lac	Boillat et al. 2020[50]
VC	visual stimulation	7 Siemens	deactivation	SPECIAL (16)	1%↓Glu, 9%↓Lac, 8%↓GABA	Boillat et al. 2020[50]
VC	visual stimulation	7 Philips	activation	sLASER (144)	3%↑Glu, 10%↑Lac	Fernandes et al. 2020[74]
left SI	sensory stimulation	3 Philips	activation	MEGA PRESS (70)	29%↓GABA	Lea-Carnall et al. 2020[99]
left M1	motor clenching	3 Siemens	activation	PR-STRESS (15)	4%↑Glu, 4%↑Glx	Volovyk and Tal 2020[65]
VC	visual stimulation	4 Bruker	activation	fMRI-fMRS: STEAM WS-MEGA sLASER (71/144)	8%↑Lac, 3%↑Glx, 6%↓GABA	Koush et al. 2021[54]
PCC	emotional recognition	4 Bruker	deactivation	fMRI-fMRS: STEAM WS-MEGA sLASER (71/144)	5%↑GABA	Koush et al. 2021[54]

TE: echo time; SE MRS: spin-echo MRS sequence; STEAM: stimulated echo acquisition mode; PRESS: point resolved spectroscopy; LASER: localization by adiabatic selective refocusing; SPECIAL: spin-echo full intensity acquired localized; JDE: J-difference editing; MEGA: Mescher Garwood JDE scheme; sLASER: semi-LASER; GE EPI: gradient-echo echo planar imaging; PR-STRESS: phase-rotated STEAM+PRESS sequence; VC: visual cortex; BG: basal ganglia including portions of putamen and globus pallidus; IFG: inferior frontal gyrus; ACC: anterior cingulate cortex; M1: sensorimotor cortex; IC: insula cortex; dlPFC: dorsolateral prefrontal cortex; MC: motor cortex; SI: primary somatosensory cortex; LOC: lateral occipital cortex; Hipp: hippocampus; PCC: posterior cingulate cortex; Glu: glutamate; Gln: glutamine; Glx: pooled Glu and Gln; mI: myo-inositol; Glc: glucose; GSH: glutathione; Gly: glycine; a/p: anterior/posterior; d/r: dorsal/rostral; activation: activation relative to baseline; activation*: expected activation relative to baseline without direct fMRI or water fMRS observations; na: non-available fMRI or water fMRS data; deactivation: deactivation relative to baseline; fMRI-fMRS: combined simultaneous fMRI and fMRS sequence; WS: water spectra.

volume are considered). Finally, spatial localization and motion correction methods in several of the early low field studies were not as effective as modern approaches, which could have led to lipid signals from outside the visual cortex contaminating the spectrum and being misinterpreted as an increase of lactate.

Reliable quantification of task-induced metabolite alterations using ^{1}H-MRS is now achievable at high fields (for review, see[20]) Moreover, advances have been to address limited spectral resolution and dispersion of chemical shifts at lower magnetic fields, extensive overlap between metabolites and lipids/macromolecules, low metabolite concentrations and small function-associated metabolite level changes all contribute to spectral quality and quantification accuracy. The basal concentrations of metabolites measured in fMRS studies to date are all in mM (or millimolar) range and include: glucose (1–2 mM), lactate (0.2–1 mM), aspartate (1–2 mM), GABA (1–2 mM), Glu (6–12.5 mM), Gln (3–6 mM), Glx (9–18.5 mM) and BHB (<0.5 mM).[9] Of note, BOLD response (seconds timescale) indirectly reflects electrophysiological processes identified by local field and/or spiking activity modulations (milliseconds timescale).[1] Similar to block design fMRI paradigms (alternating blocks of stimuli and rest periods, each lasting tens of seconds), fMRS paradigms have prolonged block designs (each block lasting minutes timescale). Prolonged block designs are demanding because of habituation effects associated with long cycling,[52] but also specific tasks can be used with limited choices of brain areas to be studied. Thereby, to ensure proper functional engagement of the target brain area(s), it is essential to justify prolonged fMRS paradigms with either identical fMRI paradigms[53] or at least with similar (typically significantly shorter) fMRI paradigms,[48,49] or alternatively, acquire concurrent fMRI-fMRS data.[54–56] Given large single fMRS voxels, conventional fMRS block designs reflect steady-state metabolite levels with low spatial resolution. Metabolic changes estimated with fMRS reflect just pooled inhibitory, excitatory and energetics effects, without possibility to separate GABAergic and glutamatergic activity unless compartmentalized metabolic models are applied.[20,54]

The ^{1}H-MRS quantification benefits from increased static magnetic field giving rise to improved chemical shift dispersion and SNR despite concomitant increase in peak linewidth (due to T_2 shortening).[9,57] However, high quality ^{1}H-MRS also requires fine adjustment of first and second order shim coils to correct for field inhomogeneities,[58–60] tissue water suppression and outer-volume signal exclusion techniques to minimize extracranial contamination from lipids and macromolecules.[8] Availability of magnetic fields at 3.0–7.0T or even higher with advanced MRI instrumentation and pulse sequence designs substantially increased ^{1}H-MRS quantification accuracy and consistency.[8,61,62] As a result of these advances, it was shown that short TE fMRS at 7.0T could provide reliable quantification of up to 20 metabolites and functional changes of up to 6 metabolites from VC in relatively small groups of 10–15 healthy participants (Figure 1(a), Table 1).[45,47,49] For comparison, short TE fMRS at 3.0T can only detect changes in glutamate or Glx.[63–65] Of note, task-induced ^{1}H-MRS spectra linewidth modulations are intrinsically sensitive to BOLD changes, which alter T_2 of both water and metabolite protons regardless of the magnetic field.[20,66–68] Although these modulations reported in fMRS literature validate expected activity, they must be compensated (Figure 1(b)).[20,49] Importantly, increased fMRS spectral quality at 7.0T also led to substantially increased temporal resolution of metabolic changes and provided the first insights into dynamics of the functional metabolic response (Figure 1(c)).[49]

The fMRS spectra at 3.0T are typically acquired with short TE (15–50ms) spin-echo point-resolved spectroscopy (PRESS) sequences.[69] At ultra-high magnetic field, PRESS sequence suffers from chemical shift displacement errors and RF (or B_1) related artifacts. Thereby ultra-short TE (6–15ms) STEAM and spin-echo full intensity acquired localized (SPECIAL) sequence[61,62] have been proposed for fMRS at 7.0T.[8,62] A more recently proposed method for high quality fMRS spectra is spin-echo full intensity sequence with semi localization by adiabatic selective refocusing (sLASER), which is characterized by reduced chemical shift displacement at ultra-high magnetic field and high test-retest reliability.[64,70] Short TE sLASER (26–40ms) has been successfully applied for fMRS at 4.0T and 7.0T.[49,53,54,56,71]

Short and ultra-short TE fMRS at various magnetic fields

Short TE (15–50 ms) and ultra-short (<15 ms) TE fMRS has been successfully applied at 3.0T and 7.0T in a variety of brain areas and tasks (Table 1). VC is often the target brain area due to easiest placement of surface RF coils despite suboptimal shimming conditions at this location. This is primarily because of relative simplicity of the stimulation required to achieve robust and sustained physiological activation, absence of task-induced body motions (e.g., as compared to intense tapping or clenching), as well as the high SNR from closer proximity to head RF coil elements.[45–47,49,50,71–73] Conventional flashing checkerboard paradigm covering whole-screen has been often used to activate VC and identified the following

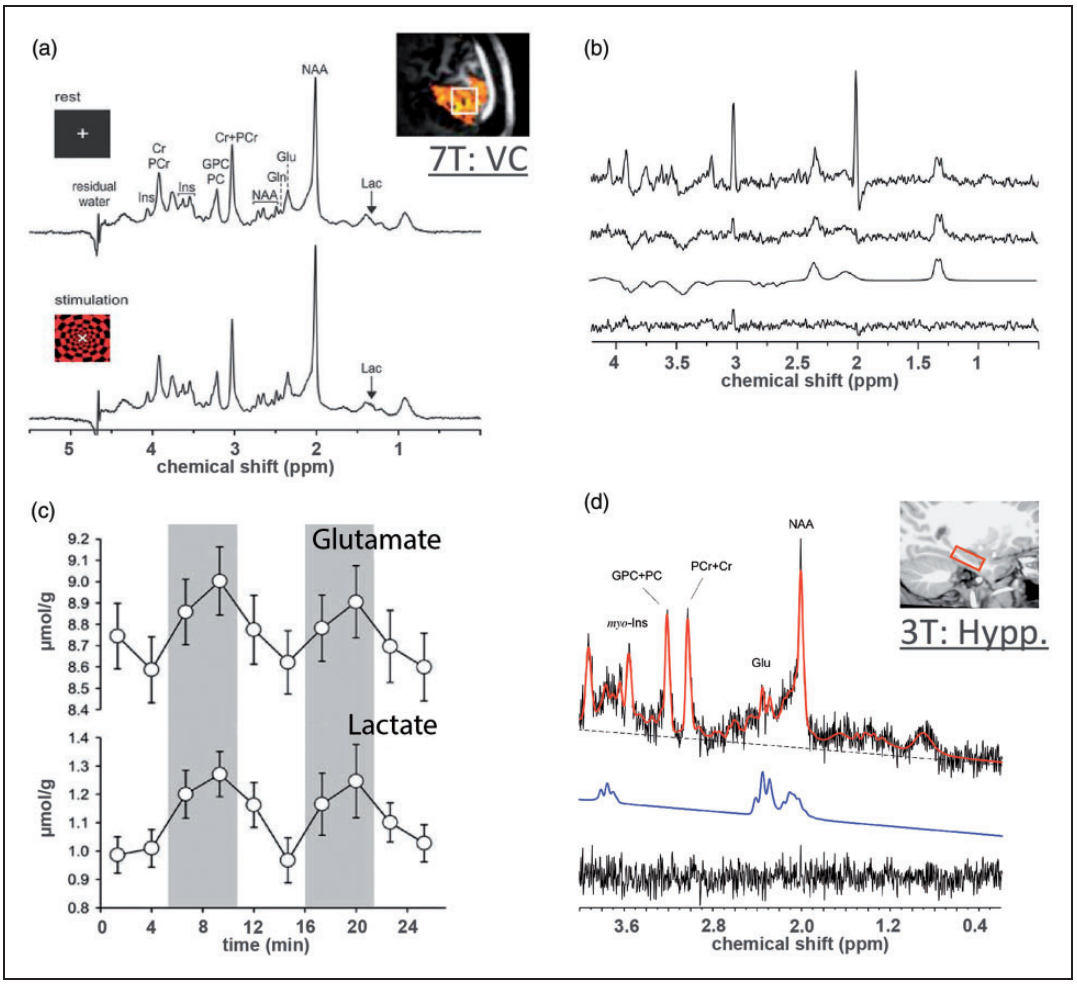

Figure 1. Short TE functional MRS in human brain at 7 T and 3 T. (a) High quality ^{1}H fMRS spectra acquired at 7 T from VC for baseline and stimulation blocks using short TE (26 ms) sLASER sequence during a flashing checkerboard task. Reliable quantification of ~20 metabolites are achievable. (b) From top to bottom, difference spectrum between stimulation and baseline blocks without compensation for BOLD line-width narrowing, difference spectrum with compensated BOLD effect, LC model fit of the difference spectrum, and fit residuals. The comparison shows that metabolite changes from short TE spectra are highly sensitive to BOLD effect change from rest to stimulation. (c) High spectra quality at 7 T allows increasing the temporal resolution of fMRS and observing task-induced dynamics of metabolic response, e.g., increases in Glutamate and Lactate. (d) Sufficient spectra quality of short TE (23 ms) PRESS sequence at 3 T allows for fMRS observations of glutamate increase associated with hippocampus activation during associative learning tasks, i.e. for a target metabolite with relatively large concentration. Panels (a–c) are modified from Bednarik et al.[49] with permission. Panel (d) is modified from Stanley et al.[80] with permission.

stimulation-induced metabolic alterations: 1.5–5% increase in glutamate, 9-30% increase in lactate, 5–15% decrease in aspartate and 12–16% decrease in glucose.[45,47,49,50,55,56,71,74] Besides, in VC, 3% increase in glutamate, 9% increase in lactate, 8% increase in glutathione, 10% decrease in aspartate, 6% decrease in glutamine and 12% decrease in glycine were observed during whole-screen moving wedges stimulation.[72] The specificity of metabolic observations during unilateral VC activation has been studied using flashing checkerboard paradigm presented only in a half of the screen for target and control regions, respectively.[73] Identified activation in contralateral to stimuli VC was associated with 7% increase in lactate and 5% decrease in GABA.

In addition to the extensively studied VC, consistent 2-4% glutamate increase, 7% glutamine increase, and 22% GABA decrease were observed in anterior cingulate cortex (ACC) during Stroop task using ultra-short TE fMRS at 3.0T and 7.0T[75–77]. Reliable 17% increase in lactate and 2% increase in glutamate were also observed in human motor cortex during finger tapping paradigm using ultra-short TE fMRS at 7.0T.[48] Conversely, motor sequence learning was found to be associated with 20% decrease of GABA in primary motor cortex, while glutamate and lactate changes

were not observed using short TE fMRS at 7.0T.[78] Of note, motor cortex fMRS has been achieved using ultra-short TE sequence at 7.0T, shifting the RF transmit B_1^+ magnetic field intensity towards target brain area by using dielectric pad placed around the subject's head, careful shimming and spectral processing procedures.[48]

Although to a lesser extent, short TE fMRS at 3.0T has been successfully used to study task-induced VC activations. Specifically, 12% glutamate increase was observed during visual repetition-priming cognitive task,[79] and 50% lactate increase was observed during flashing checkerboard stimulation.[30] Consistently, short TE fMRS at 3.0T unveiled: 4–11% glutamate increases in hippocampus during associative learning tasks (Figure 1(d));[80] 18% glutamate increase in insular cortex during acute heat pain applied to the left forearm;[81] 13–16% Glx increase, 6–55% glutamate increase, 20–32% glutamine increase, and 6–13% myo-inositol decrease in insular cortex during dental pain induced by electrical stimulation;[82,83] 12% glutamate increase in lateral occipital cortex after novel visual stimuli presentation;[84] and 3% glutamate increase in dorsolateral prefrontal cortex during working memory task.[85] In addition, the heat pain applied to the right upper leg was associated with 15% GABA increase in rostral ACC as identified by short TE fMRS at 3.0T,[86] as well as heat pain applied to the forearm was associated with 2% glutamate decrease in dorsal ACC as identified by ultra-short TE fMRS at 3.0T.[87]

These studies show that, regardless of the region and type of stimulation, activation paradigms reproducibly lead to increased levels of glutamate and lactate, with a commensurate decrease in glucose. These can largely be interpreted as heightened metabolic demands to support neuroenergetics and neurotransmission. However, verification of the potential involvement of a few other less frequently observed metabolites reported during (de)activation (e.g., myo-inositol, glycine, glutathione, BHB) will be technically challenging, and best addressed at ultra-high magnetic field.[57,88]

J-difference edited fMRS at various magnetic fields

While short TE MRS at 3.0T has shown variable fMRS results, fMRS observations at 7.0T are largely consistent across metabolite changes implicated in neuroenergetic (glucose, lactate) and neurotransmission (glutamate, GABA). Fortunately, these metabolic changes can also be detected by J-difference editing (JDE) ^{1}H-MRS at lower magnetic fields. Spectral editing with J modulation takes advantage of the quantum mechanical properties of specific molecules to selectively observe or "edit" them from the overall ^{1}H-MRS spectrum,[89] thereby providing separation from overlapping resonances and lipids/macromolecules. Advantage of an edited signal over non-edited signal detection is strongly dependent on the molecule of interest and magnetic field strength. The ultimate goal of spectral editing, including JDE, is to reduce the dynamic range between a signal-of-interest (e.g., GABA) and partially overlapping signals (e.g., creatine). For GABA at low magnetic fields the removal of creatine by JDE is so pronounced that detection error (as for example measured by Cramer-Rao lower bound (CRLB) fitting) on GABA greatly decreases. Thus, in such cases use of spectral editing is mandatory. At higher magnetic fields, like 7.0T and above, the overlap between creatine and GABA is partial so that GABA may be detected with direct, non-edited ^{1}H MRS. However, even at high magnetic fields the use of JDE can still be beneficial as the CRLB of a non-overlapping signal is always lower than that of a partially overlapping one, provided that the decrease in detection sensitivity due to the longer TE does not undue SNR gains achieved by editing. With JDE spectrum contains the scalar couplings, but also the distorted portion where the frequency-selective editing pulses are applied. While JDE gives a superior depiction of the "edited" signal, other portions of the spectrum cannot be relied upon. Although the water signal should be edited out in the JDE spectrum, typically a non-zero water signal is observed which arises due to small variations in vasomotion, frequency drift, RF coil loading that lead to minute water subtraction errors between the two experiments for JDE. Thus, JDE still requires excellent water suppression to reduce water-related distortions in the JDE spectrum.

JDE MRS is typically based on the MEscher-Garwood (MEGA) J-editing scheme,[90] during which selective refocusing pulses are applied at the coupling partner of the target spin system (editing ON) and at the mirror position (editing OFF) relative to the water frequency or relative to the target spin system. Frequency selective editing pulse refocuses the evolution of scalar coupling of target spin system in the editing ON experiment, whilst during editing OFF it remains unaffected. Then, the sum and difference between editing OFF and ON experiments correspond to spectra of J-edited sum that contains resonances of unaffected signals and J-edited difference that contains resonances of affected signals, respectively (Figure 2(a) for MC, motor cortex, and (b,c) for VC and PCC, posterior cingulate cortex). JDE MRS is based on scalar coupling evolution which requires a longer TE, which is optimized for specific spin systems to maximize the amount of editing, typically ranging 70–200 ms. Besides, JDE MRS could be used to co-edit additional

metabolites that have similar J-evolution profiles with a target metabolite and captured by bandwidth of the applied refocusing pulse.[9,91] Typically, pooled glutamate and glutamine (termed Glx) at 3.75 ppm is co-edited with GABA at 3.01 ppm in GABA JDE fMRS spectra,[54,92–94] and similarly BHB at 1.19 ppm is co-edited with lactate at 1.31 ppm in lactate JDE fMRS spectra[53,54] (Figure 2).

GABA measured by JDE fMRS has been shown feasible to reliably detect metabolic changes in different brain areas at 3.0T and 7.0T (Figures 2 and 3). Most consistently at 3.0T, GABA decrease and Glx increase were observed in ACC (22% Glx increase and 15% GABA decrease) and VC (16% Glx increase and 13% GABA decrease) during acute heat pain applied to the left forearm,[94] as well as in VC activation during eyes-open and flashing checkerboard stimulation tasks in darkness as compared to eyes-closed (10% Glx increase and 20% GABA decrease).[93] Of note, the edited GABA signal at 3.0T includes co-edited lipids/macromolecules.[92,95,96] Hence, assuming no change in lipids/macromolecules with task, the reported task-related GABA changes typically underestimate true changes of inhibitory tone. GABA JDE fMRS was used to study VC activation during flashing checkerboard stimulation and PCC deactivation during auditory emotion identification (VC: 3% Glx increase and 6% GABA decrease; PCC: 5% GABA increase) at

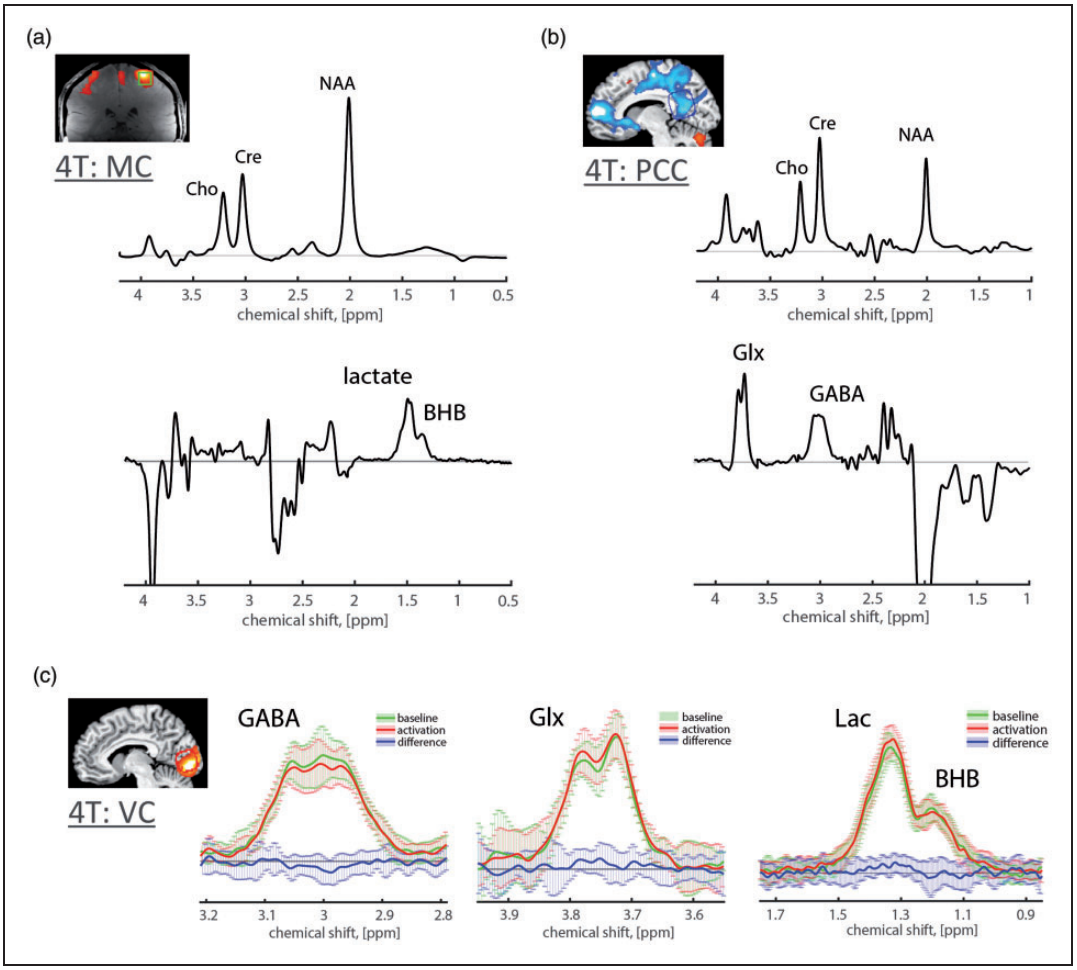

Figure 2. J-difference edited fMRS in human brain at 4 T. JDE ^{1}H MRS allows for high quality spectra observations of such low concentration metabolites as Lac (0.2–1 mM), pooled Glu (6–12.5 mM) and Gln (3–6 mM) termed as Glx, GABA (1–2 mM) and BHB (<0.5 mM) using MEGA-PRESS or MEGA-sLASER sequences at relatively low magnetic field (Table 1). For baseline condition, conventional group (a) average motor cortex (MC) JDE sum spectra for Lac JDE (TE = 144 ms) and (b) average posterior cingulate cortex (PCC) JDE spectra for GABA/Glx JDE (TE = 71 ms) using MEGA-sLASER sequence at 4 T.[53,54] Note that the difference GABA spectrum contains flipped NAA peak due to the subtraction between the NAA amplitude-distorted spectrum (by the editing ON pulse applied adjacent to NAA) and editing OFF spectrum with unaffected NAA peak. (c) For flashing checkerboard paradigm at 4T, group average J-difference spectra for activated VC baseline (green), condition (red) and their difference (blue; decrease in GABA $-5.7 \pm 3.3\%$ from baseline level 2.22 ± 0.33 mM, increase in Glx $3.0 \pm 2.1\%$ from baseline level 1.50 ± 0.21 a.u., increase in Lac $7.8 \pm 5.4\%$ from baseline level 0.99 ± 0.13 mM, and no changes in BHB).[54] Shaded error bars denote standard deviation.

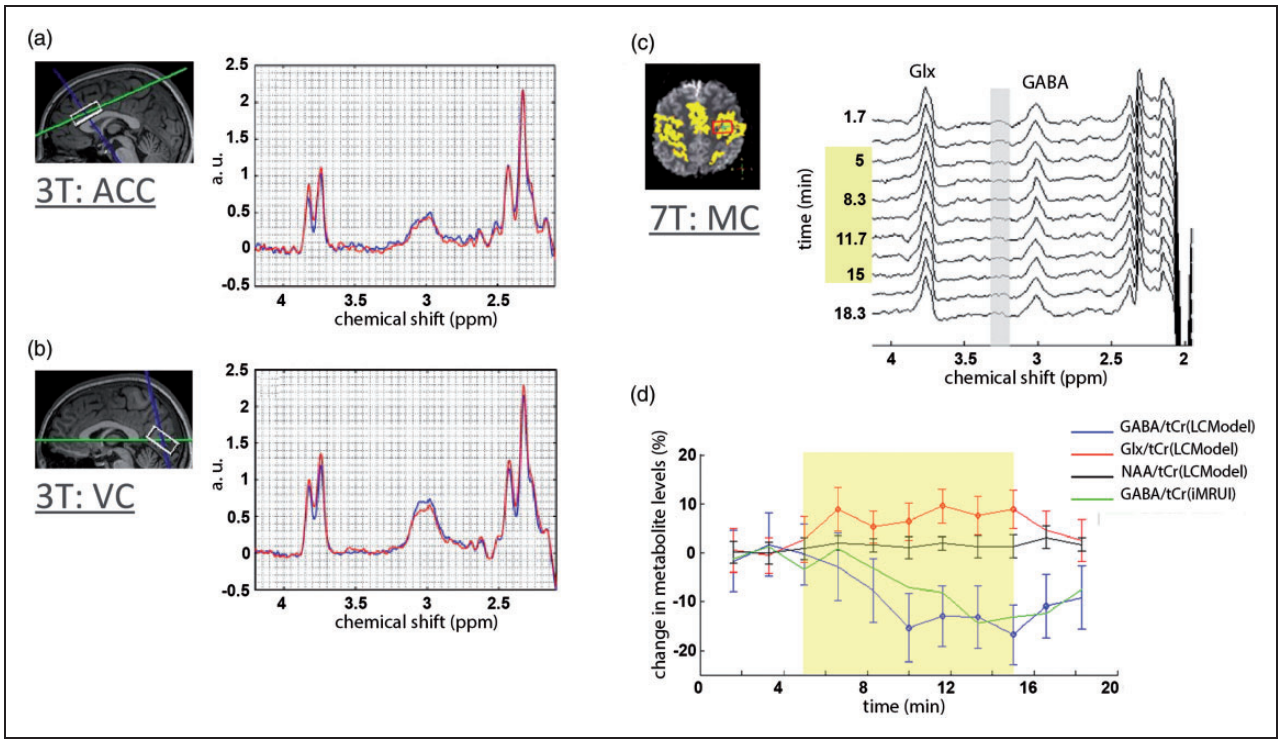

Figure 3. J-difference edited fMRS in human brain at 3T and 7T. (a,b) Group average anterior cingulate cortex (ACC) and visual cortex (VC) GABA/Glx JDE spectra highlight an increase of Glx and a decrease of GABA during acute forearm heat pain paradigm using MEGA-PRESS sequence (TE = 68 ms; blue baseline and red pain state spectra) at 3T.[94] (c) Group average motor cortex (MC) GABA JDE spectra during hand clenching paradigm using MEGA-sLASER sequence (TE = 72 ms) at 7T.[92] (d) The time-course of the group average MC spectra and (d) block-related group average MC spectra obtained during the hand-clenching paradigm highlight improvement in the temporal resolution of JDE fMRS at 7T.[92] Panels (a,b) are modified from Cleve et al.[94] with permission. Panels (c,d) are modified from Chen et al.[92] with permission.

4.0T.[54] In addition, 20% GABA decrease was observed following repetitive sensory stimulation of two fingertips in primary sensorimotor cortex,[97] 18% GABA decrease was observed during threat of shock condition in medial prefrontal cortex,[98] 29% GABA decrease was observed during motor learning task in primary somatosensory cortex,[99,100] 4% GABA increase was observed during working memory task in dorsolateral prefrontal cortex,[101] as well as 22% GABA decrease was observed during Stroop task in ACC.[77] Recently, GABA JDE fMRS has been shown feasible at 7.0T, retaining good SNR for measuring dynamic changes of GABA and Glx. It was used to study motor cortex activation during hand clenching and revealed 11% Glx increase and 12% GABA decrease.[92]

Most recently, lactate JDE fMRS at 4.0T has also been used to study task-induced modulations during motor cortex activation using finger tapping (9% lactate increase),[53] during VC activation using flashing checkerboard (8% lactate increase)[54] and during PCC deactivation using auditory emotion identification (no lactate changes).[54] In these studies, the presence of lactate co-edited BHB was consistent in the JDE spectra from visual (0.34 mM), motor (0.28 mM) and posterior cingulate (0.34 mM) cortices, although no significant task-induced BHB level changes were detected given applied experimental conditions at 4.0T. Of note, JDE fMRS of lactate utilizes long TE (144 ms) that results in reduction of macromolecular contributions to lactate spectra due to dephasing of macromolecule signal. This facilitates determination of lactate changes as compared to short TE fMRS spectra where accurate deconvolution of low concentration metabolites from overlapping resonances remains a significant challenge for identification of basal lactate levels. Conversely, JDE MRS is compromised with long TE that may lead to some T_2 signal losses, with the editing pulse flip angle and chemical shift displacement, factors which do not affect the short TE fMRS. Nevertheless, highlighted studies show that, regardless of the region and type of stimulation, JDE fMRS is capable of consistent detection of functional modulations in GABA, Glx and lactate at 3.0T, 4.0T and 7.0T magnetic fields.

Interpreting ^{1}H fMRS findings of metabolite changes

In this section we focus on interpretations of most consistent fMRS observations in lactate, glutamate/Glx and GABA (Table 1). Task-induced decreases of glucose are believed to reflect increased CMR_{Glc} in response to increased energy demands and net glucose influx through blood-brain barrier. Since lactate is an end product of aerobic glycolysis, glucose decrease and lactate increase are expected in fMRS activation studies. However, short and ultra-short TE fMRS at 7.0T is not always sensitive to significant glucose changes, most likely due to its spread of glucose resonances, small glucose concentration, an overlap with other strong resonances, as well as due to the suboptimal experimental conditions.[47–49,57,71,72] Task-induced increases in both glutamate and lactate are typically considered to reflect increases in CMR_{O2} and CMR_{Glc}. However, they are complicated to interpret due to their reflecting coupled changes in both neurotransmitter and other metabolic fluxes.[2,102,103] In particular, lactate increase is complicated by the fact that it can indicate a rise in non-oxidative glycolysis,[2,22,104] the debate about degree of lactate compartmentalization in neurons vs. astrocytes and lactate shuttling between neurons and astrocytes,[34,36] and possible action of lactate as a blood volume neurotransmitter mediating vasodilation.[28,35] Regardless of these remaining questions, task-induced lactate and glutamate/Glx changes have been shown to correlate positively with BOLD signal changes.[49,54,55,93,105]

Glutamate is a major excitatory neurotransmitter and a precursor of GABA.[102,106,107] It is directly linked to the TCA and energy metabolism,[102,108] suggesting that energetic and glutamatergic changes could be paralleled in activated brain areas.[20,49,54] Consistent increase of glutamate and decrease of aspartate have been observed during VC stimulation using fMRS at 7.0T[45,49,71,72] (Table 1), which could be associated with the increased rate of the malate-aspartate shuttle (MAS) and increased flux into the TCA cycle during stimulation.[20,109] MAS maintains the cytosolic redox potential required for glucose utilization and neurotransmitter synthesis.[109] In one fMRS study, increase of glutamate during visual stimulation was coupled with an expected decrease of glutamine underlying an increased flux of the glutamate-glutamine cycle.[72] Glutamate-glutamine cycle could balance impermeable to blood-brain barrier stimulation-induced glutamate changes to prevent ecotoxicity, thus reflecting concomitant modulation of glutamine.[110]

GABA is a major inhibitory neurotransmitter and tissue GABA as measured by ^{1}H fMRS reflects mainly intracellular GABA as extracellular GABA is too low for detection. Because intracellular GABA determines extracellular GABA as maintained by plasma membrane GABA transporters which operate near equilibrium, task-induced GABA alterations can reflect changes in extracellular GABA level, and thus in tonic inhibition. Activation-induced GABA level decreases were observed during motor and sensory stimulation,[78,97,99] as well as GABA decrease together with lactate/glutamate/Glx increase were observed during visual, motor and pain stimulation[54,73,92–94] (Table 1). Also, GABA could alter local CBF and hence the BOLD response via release of vasoactive neuromodulators such as intestinal peptide from inhibitory neurons.[111]

Less commonly, increased GABA levels have been observed during activations in certain brain areas (Table 1). Activation of dorsolateral prefrontal cortex during a working memory task has been shown to be associated with parallel increases of GABA[101] and Glu.[85] Activation of rostral ACC during heat pain stress was associated with an increase of GABA and suggested to represent an increased inhibition of pain-induced excitatory thalamo-cingulate afferent input.[86] In dorsal ACC during reinforcement learning, activation led to a 3–10% increase of GABA, potentially reflecting increased inhibition during high cognitive load.[112] Vigorous physical exercise on a bicycle ergometer was associated with 3–7% glutamate increase and 7% GABA increase in VC, 5% glutamate increase in rostrodorsal ACC[113] as well as with 18% Glx and 19% lactate increase,[114] suggesting exercise-induced expansion of cortical pools of lactate, glutamate and GABA.

In addition to studying localized brain activations as compared to baseline, fMRS has been recently used to study localized deactivations[50,54,105] (Table 1). Although these findings are heterogenous across observed deactivation-induced metabolic changes, target brain areas and experimental conditions, they are consistent in that localized deactivation could be mediated by metabolic alterations different from those underlying localized activation. Since deactivation is not simply the inverse of activation, metabolism may differ across deactivated brain areas/tasks.[50,54] Interestingly, deactivation of rostral ACC was found to be associated with 2% Glx level increase during mental imagery task.[115] Furthermore, along with whole-screen flashing checkerboard activations in VC described above, a centered, small-circle flashing checkerboard was used to deactivate VC. This deactivation was associated with 8% decrease in glucose, 4% decrease in glutamate and 4% increase in glutathione,[105] as well as with 1.3% decrease in glutamate, 9% decrease in lactate and 8% decrease in GABA.[50] One of the key distinctions between these studies was

either different[105] or identical[50] VC areas used for activation and deactivation during fMRS. In addition, more metabolic alterations were observed by Boillat et al,[50] which could be due to the larger sensitivity of the applied ultra-short TE (16 ms) SPECIAL sequence as compared to the short TE (40 ms) sLASER sequence used by Martinez-Maestro et al.[105] Nevertheless, both studies consistently show decreased glutamate level during deactivation, suggesting decreased TCA cycle activity as compared to baseline, which is paralleled by decreased lactate level suggesting an overall reduction in CMR_{Glc} and neuronal activity.[50] Boillat et al.[50] suggested that the significant decrease in GABA during VC deactivation may be paralleled with glutamate decrease as it is a GABA precursor.[102,106,107] Since fMRS measured changes in GABA and glutamate are believed to reflect GABAergic and glutamatergic neurons, the concurrent change of both neuronal pools is difficult to interpret. Conversely, functional rise of aerobic glycolysis (lactate increase) and glutamatergic activity (glutamate increase) was found to be specific to the activation in VC during whole-screen flashing checkerboard stimulation and not to the deactivation in posterior cingulate cortex during auditory emotion identification.[54] In addition, VC activation was associated with 6% GABA decrease, and PCC deactivation was associated with 5% GABA increase.[54] These findings suggest that neurotransmission in VC and PCC differ in terms of their support by aerobic glycolysis during activation and deactivation as compared to baseline, possibly through differences in the modes of neurotransmission and/or neuroenergetic capabilities. For smaller absolute changes in signaling in PCC, these findings do not exclude the possibility that detection sensitivity was not sufficient to see a significant decrease in Glx, or that small glutamate changes were counter-balanced by opposite changes in glutamine in pooled Glx observations. Moreover, an opposite effect of larger task-induced GABA changes in activated (negative correlation with BOLD response) and deactivated (positive correlation with BOLD response) brain areas was observed.[54] More detailed interpretations of (de)activation mechanisms are available in the original publications.[50,54,105]

Given the sparseness of fMRS studies investigating BHB changes, some caution is necessary for interpreting these studies in the context of the others being reviewed for other metabolites. BHB concentration can rise substantially due to prolonged exercise[116] and fasting,[117] and serve as an additional substrate to partly fulfill energy demands in the presence of low glucose.[118] However, its potential role in functional activation has not been addressed so far due to the limited sensitivity and very low BHB concentration (<0.5 mM). Lactate JDE MRS demonstrated sufficient sensitivity for the BHB quantification at 4.0T[53,54] and 3.0T,[119] but the accuracy to determine BHB change was insufficient; thus mandating additional investigation, e.g. at 7.0T. Therefore, we suggest that BHB could serve as an additional, not alternative, energy source to meet exceedingly high energy demand situation.

Overall, these studies show that levels of glutamate (or Glx) and GABA can change in opposite directions during brain activation, suggesting that a new excitatory/inhibitory balance is integral to the neuropil activating process. In contrast, metabolite changes associated with deactivation processes are more heterogenous and require further investigation.

Interpreting ^{1}H fMRS findings of metabolite levels

With functional metabolic alterations, basal levels of excitatory and inhibitory neurotransmitters are implicated in modulation of local brain responses to activation and deactivation stimulations and tasks, and functional/effective connectivity during task and/or resting-state conditions (Table 2). For the same brain area, regional resting-state GABA level modulates inter-subject BOLD response variability so that greater inhibition is associated with smaller positive BOLD magnitude (activation) in VC during visual stimulation,[49,54,93,120–122] in anterior temporal lobe (ATL) during semantic processing,[123] and in left primary sensorimotor cortex during motor learning.[124] In addition, higher individual resting-state GABA level is associated with larger negative BOLD magnitude (deactivation) in rostral ACC during emotion processing,[125,126] in PCC during working memory task[127] and during auditory emotion identification task,[54] as well as in medial PFC during working memory task.[128] For different brain areas, higher individual resting-state GABA level in dorsal ACC is associated with greater amygdala activation during fear recovery and deactivation during fear extinction.[129] Since the inverse relationship between tissue GABA level and BOLD response extends over both activated and deactivated areas (Table 2), the fMRS GABA measure reflects a common inhibitory effect modulating excitation-inhibition balance, suggesting that basal inhibition of brain activity is ubiquitously important for normal brain function.[54]

The relationship between resting-state glutamate (Glx) and local BOLD response and/or connectivity between brain areas/networks is less prominent than for GABA (Tables 2 and 3). For the same brain area, higher individual resting-state glutamate (Glx) was associated with more deactivation in pregenual ACC

Table 2. Combined fMRI and MRS for various brain regions shows correlations between basal GABA/Glx/glutamate level and fMRI signal.

area	task	Bo (T) Vendor	fMRS sequence (TE, ms)	metabolite	fMRI	correlation	reference
pregACC	emotion processing	3 Philips	JPRESS (31-229)	GABA	deactivation	negative	Northoff et al. 2007[125]
pregACC	emotion processing	3 Philips	JPRESS (31-229)	GABA	deactivation	negative	Walter et al. 2009[126]
VC	visual stimulation	3 GE	MEGA PRESS (68)	GABA	activation	negative	Muthukumaraswamy et al. 2009[120]
VC	visual stimulation	3 Siemens	MEGA PRESS (69)	GABA	activation	negative	Donahue et al. 2010[121]
left M1	reaction time task	3 Siemens	MEGA PRESS (68)	GABA	activation	negative	Stagg et al. 2011[124]
VC	visual stimulation	3 GE	MEGA PRESS (68)	GABA	activation	negative	Muthukumaraswamy et al. 2012[122]
perigACC	reward delay	3 Siemens	PRESS (80)	Glx	deactivation	negative	Enzi et al. 2012[130]
PCC	working memory	3 Siemens	MEGA PRESS (68)	GABA	deactivation	negative	Hu et al. 2013[127]
PCC	working memory	3 Siemens	MEGA PRESS (68)	Glu	deactivation	positive	Hu et al. 2013[127]
VC	visual stimulation	7 Siemens	sLASER (26)	GABA	activation	negative	Bednarik et al. 2015[49]
left ATL	semantic processing	3 Philips	MEGA PRESS (68)	GABA	activation	negative	Jung et al. 2017[123]
VC	visual stimulation	3 Siemens	MEGA PRESS (68)	GABA	ALFF	negative	Kurcyus et al. 2018[93]
VC	visual stimulation	3 Siemens	MEGA PRESS (68)	Glx	activation	positive	Kurcyus et al. 2018[93]
mPFC	working memory	3 Siemens	MEGA PRESS (68)	GABA	deactivation	negative	Chen et al. 2019[128]
VC	visual stimulation	4 Bruker	MEGA sLASER (71)	GABA	activation	negative	Koush et al. 2021[54]
PCC	emotion recognition	4 Bruker	MEGA sLASER (71)	GABA	deactivation	negative	Koush et al. 2021[54]

ACC: anterior cingulate cortex; VC: visual cortex; M1: sensorimotor cortex; PCC: posterior cingulate cortex; ATL: anterior temporal lobe; pmC: posteromedial cortex; dlPFC: dorsolateral prefrontal cortex; mPFC: medial prefrontal cortex; preg: pregenual; perig: perigenual; activation: activation relative to baseline; deactivation: deactivation relative to baseline; ALFF: amplitude of low-frequency fluctuations; JPRESS: J-resolved PRESS.

Table 3. Combined fMRI and MRS for various brain regions shows correlations between basal GABA/Glx/glutamate level and functional connectivity estimates.

area	task	Bo (T) Vendor	fMRS sequence (TE, ms)	metabolite	connectivity	correlation	reference
perigACC	emotion processing (EO)	3 Siemens	PRESS (80)	Glx	perigACC-supragACC	associated	Duncan et al. 2011[131]
dACC	resting-state (EC)	3 Philips	PRESS (38)	Glu	dACC-midbrain/PCC	positive	Schmaal et al. 2012[140]
pmC	resting-state (EO)	3 Philips	JPRESS (31-229)	Glu	DMN strength	positive	Kapogianis et al. 2013[133]
pmC	resting-state (EO)	3 Philips	JPRESS (31-229)	GABA	DMN strength	negative	Kapogianis et al. 2013[133]
mPFC	resting-state (EO)	3 Siemens	MEGA PRESS (68)	Glu	mPFC-Nac/dmTh	positive	Duncan et al. 2013[139]
mPFC	resting-state (EC)	3 Siemens	MEGA PRESS (68)	Glu	mPFC-PAG	negative	Duncan et al. 2013[139]
PCC	resting-state (EC)	3 Siemens	PRESS (14/105)	GABA	putamen-DMN	negative	Arrubla et al. 2014[134]
left M1	resting-state (EO)	3 Siemens	MEGA PRESS (68)	GABA	motor RSN strength	negative	Stagg et al. 2014[136]
Striatum	resting-state	3 Philips	MEGA PRESS (68)	GABA	BGN strength	positive	Haag et al. 2015[137]
left M1	resting-state (EO)	3 Siemens	MEGA PRESS (68)	GABA	motor RSN strength	negative	Bachtiar et al. 2015[135]
dACC	fear recovery (EO)	3 Philips	MEGA PRESS (73)	GABA	AMY-vmPFC	negative	Levar et al. 2017[129]
dACC	fear extinction (EO)	3 Philips	MEGA PRESS (73)	GABA	AMY-vmPFC	positive	Levar et al. 2017[129]
mPFC	resting-state (EC)	3 Philips	MEGA PRESS (68)	GABA	AMY-vmPFC	negative	Delli Pizzi et al. 2017[138]
mPFC	working memory	3 Siemens	MEGA PRESS (68)	GABA	mPFC-dlPFC	negative	Chen et al. 2019[128]
mPFC	resting-state	3 Siemens	MEGA PRESS (68)	GABA	mPFC-dlPFC	negative	Chen et al. 2019[128]

ACC: anterior cingulate cortex; pmC: posteromedial cortex; M1: sensorimotor cortex; PFC: prefrontal cortex; PCC: posterior cingulate cortex; AMY: amygdala; PAG: periaqueductal grey; DMN: default mode network; RSN: resting-state network; BGN: basal ganglia network; Nac/dmTh: nucleus accumbens/dorsomedial Thalamus; perig: perigenual; suprag: supragenual; vm: ventromedial; dl: dorsolateral; d/m: dorsal/medial; EO: eyes-open; EC: eyes-closed.

during monetary reward incentive delay task,[130] with less deactivation in PCC during working memory task,[127] and with more activation in VC during visual stimulation.[93] In addition, for different brain areas, higher individual perigenual ACC resting-state Glx is associated with larger activation in subgenual ACC during emotional faces viewing.[131] Individual variability of resting-state dorsal ACC glutamate is related to cognitive control.[132] Specifically, lower individual glutamate levels are associated with higher BOLD response in retrosplenial cortex, orbitofrontal cortex, inferior parietal lobe, and basal ganglia during high-demand dichotic listening. Conversely, higher glutamate levels are associated with larger BOLD response in the same brain areas during low-demand dichotic listening.

In additional to local BOLD responses, inter-individual resting-state GABA and glutamate levels are associated with functional connectivity estimates between specific brain areas, within resting-state networks and between different networks. Inter-individual resting-sate GABA levels in posteromedial cortex correlated negatively with functional connectivity strength of default mode network, DMN,[133] and GABA levels in PCC correlated negatively with the connectivity strength between putamen and DMN.[134] In sensorimotor cortex (M1), GABA level correlated negatively with the connectivity strength of motor resting-state network (RSN),[135,136] whereas in striatum, GABA level correlated positively with the connectivity strength of basal ganglia network (BGN).[137] Inter-individual resting-state GABA levels in dorsal ACC correlated negatively with effective connectivity strength between amygdala and deactivated ventromedial PFC during fear recovery and correlated positively with effective connectivity strength between amygdala and activated ventromedial PFC during fear extinction, as assessed by psychophysiological interaction (PPI).[129] Inter-individual resting-state GABA level in medial PFC correlated negatively with anti-correlation between dorsomedial PFC, the DMN node, dorsolateral PFC and the control network (CN) node during rest and during working memory task.[128] In addition, inter-individual resting-state medial PFC GABA levels correlated negatively with negative functional coupling between amygdala and ventromedial PFC.[138]

Inter-individual resting-state glutamate levels in medial PFC correlated positively with functional connectivity between medial PFC and nucleus accumbens (NAc) and between medial PFC and dorsomedial thalamus (dmTh), as well as correlated negatively with functional connectivity between medial PFC and periaqueductal grey (PAG).[139] In dorsal ACC, glutamate correlated positively with functional connectivity between dorsal ACC and midbrain and between dorsal ACC and PCC,[140] while in posteromedial cortex glutamate correlated positively with functional connectivity strength of DMN.[133] Inter-individual resting-state glutamate levels in perigenual ACC have been implicated in the interaction (effective connectivity assessed using PPI) between task-negative perigenual ACC and task-positive supragenual ACC during emotion processing task.[131]

In summary, these studies show that, regardless of the region and type of stimuli, basal tissue levels of glutamate (or Glx) and GABA impact the BOLD response reciprocally, suggesting that the resting tissue levels may reflect their excitatory and inhibitory neurotransmitter levels underlying brain activity, connectivity and the reproducibility of BOLD changes. Further investigations that link the MRS measurement of tissue glutamate and GABA to their neurotransmitter levels are critically needed.

J-edited difference MRS advances for multiple metabolites and brain areas

Conventional JDE MRS targets a single metabolite of interest at a single brain location and time, which could require 8-10 min per experimental observation/condition, substantially limiting the number of target metabolites per fMRS experimental session. An approach that bypasses this limitation is the use of Hadamard encoding,[141] which facilitates efficient MRS data acquisition. When applied to multivolume/multifrequency localizations, Hadamard encoding substantially reduces total scan time without compromising SNR.[9] It can be used with spectral editing when applied to frequency selective refocusing pulses given single voxel localization, such as PRESS, sLASER and SPECIAL.[142] For example, Hadamard Encoding and Reconstruction of MEGA-Edited Spectroscopy (HERMES) allows simultaneous detection of two spin systems by acquiring four experiments with different combinations of editing pulses: (A) ON, ON; (B) ON, OFF; (C) OFF, ON; and (D) OFF, OFF (Figure 4(a)).[143] The acquired data are then combined (A–B + C–D and A + B – C – D) to separate overlapping resonances without compromising SNR and scan time, as compared to sequential JDE MRS for individual molecules. HERMES was used to separate GABA and glutathione,[142,144] and N-acetylaspartate (NAA) and N-acetylaspartylglutamate (NAAG).[143] Also, it has the potential to segregate more than two target spin systems with comparable quality to MEGA-PRESS JDE spectra, under the condition that the target resonances are separated by more than the bandwidth of the editing pulses, such as the ^{1}H resonances of NAA, NAAG and aspartate molecules.[143] The

A + B + C +D combination consists of spectra at full SNR, largely unaffected by editing pulses and can be used for whole-spectrum quantification. HERMES results in co-editing of molecules, like that of MEGA-PRESS, providing Glx in the GABA-glutathione JDE spectrum. To segregate multiple low concentration metabolites at 3.0T, a Hadamard-encoded editing scheme was combined with multiplexed linear-modeling using simulated basis functions, i.e., Hadamard editing resolves chemicals using linear-combination estimation of spectra (HERCULES).[145] The HERCULES editing scheme is based on four experiments (TE = 80 ms) and combinations of three editing pulses at 1.9 ppm (targeting GABA and 2-hydroxyglutarate), 4.18 ppm (targeting ascorbate, aspartate, lactate), and 4.58 ppm (targeting glutathione and NAAG). Three spectral combinations, A + B + C +D, A–B + C–D, A + B – C – D, are quantified simultaneously. Thus, the HERCULES technique allows for the quantification of multiple coupled metabolites in the same scan time that would be required for segregation of a single metabolite. Specifically, the quantified metabolites include ascorbate, aspartate, GABA, glutathione, NAAG and lactate along with choline, creatine, myo-inositol, glutamate, glutamine, 2-hydroxyglutarate (elevated in some tumors), and co-edited Glx. Note that 2D J-resolved spectroscopy (2D JRES)[146] detects various scalar coupling resonances and has been successfully used to study associations between localized GABA levels and BOLD response.[125] However, besides the required longer acquisition time that does not fit the typical fMRS block design, the resolving power of in vivo 2D JRES is limited in, e.g., resolving GABA from creatine and macromolecules. When focused on a single metabolite (e.g., GABA) the use of JDE is recommended, whereas JRES is more appropriate to establish an entire steady-state metabolic profile.

There are intense efforts to improve spatial information content of JDE MRS and to accelerate acquisition, which could be achieved by extending the number of simultaneously scanned voxels and by incorporating the JDE MRS advances in the MRS imaging (MRSI) pulse sequences. Specifically, parallel reconstruction in accelerated multivoxel (PRIAM) MRS has been developed as a means of extending the conventional single-volume MEGA-PRESS sequence to a dual-volume sequence by incorporating dual-band excitation pulses and parallel reconstruction (Figure 4 (b)).[147] Applied parallel reconstruction was based on the spatial sensitivity encoding of the multichannel phase-array coil (SENSE).[148] SENSE reconstruction performs well for multichannel coils, as compared to coils with fewer channels, due to the less overlap between sensitivity profiles of the receive coil elements. SENSE cannot be performed for single-channel receive coils. To overcome this limitation, spatial Hadamard encoding has been implemented for the dual-voxel

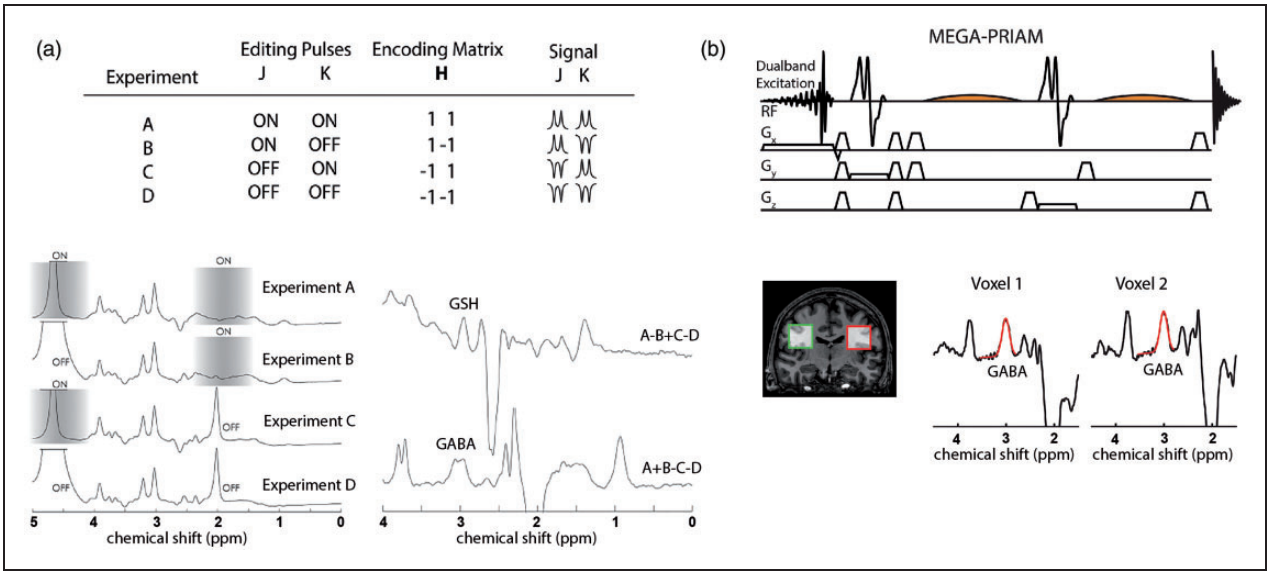

Figure 4. Methodological advances for JDE MRS in the human brain. (a) Single-subject Hadamard encoded JDE spectra with four step J-editing scheme of applied frequency-selective pulses (shaded grey blocks) for two target molecules. The combination of Hadamard experiments efficiently separates overlapping GABA and GSH resonances. (b) Simultaneous acquisition of JDE spectra from two simultaneously excited voxels has been shown feasible at 3T using a combination of MEGA-PRESS JDE with parallel reconstruction of accelerated multivoxel (PRIAM) acquisitions. Panel (a) is modified from Chan et al.[143] and Saleh et al.[142] with permission. Panel (b) is modified from Oeltzschner et al.[147] with permission.

localization by applying gradient pulses during frequency-selective editing pulses.[149] This method could be used both for single- and multichannel receive coils without SNR loss and coil geometry limitation. The placement of voxels in dual-voxel localization approaches is limited by a few factors, namely, editing efficiency linked to editing frequency and distance between voxels, single-slice dual-band excitation, voxel geometry and suboptimal shimming of an area covering both voxels, which could be compromised by reasonable voxel placement and methodological advances such as multiband slice-selective pulses and separate voxel shimming.[147,150] Importantly, spatial acceleration based on multivolume approaches could be combined with Hadamard encoding schemes for multiple metabolites, such as HERMES and HERCULES. It has also been suggested that multivoxel MRS acquisitions can be greatly accelerated by combining PRIAM and HERMES for improved MRS efficiency.[147] In addition, spatial GABA acquisitions were performed using MEGA LASER JDE with spiral-encoded 3D-MRSI at 3.0T[151] and GABA-glutathione MEGA PRESS using HERMES editing with MRSI at 3.0T,[152] which is a promising approach for mapping multiple low concertation metabolites (for studies on JDE MRS and MRSI methods, see reviews[153,154]) The feasibility of detecting lactate functional changes using a single voxel, long TE (144 ms) sLASER sequence has been recently demonstrated for VC during visual stimulation at 7.0T (Figure 5).[74] This method is similar to the editing OFF experiment in lactate JDE MRS,[53,54,119] however, it benefits from the high quality sLASER localization at ultra-high magnetic field as compared to the long TE fMRS studies.[31,38,42,43]

Combined fMRI-fMRS and real-time water proton fMRS

Functional changes in low SNR metabolites of low concentration can be consistently interpreted if the concomitant BOLD response is measured in the selected spatial location, experimental design and tasks. In most fMRS studies, whole-brain fMRI is used as localizer to identify individual brain (de)activation clusters for placement of the single fMRS voxel. In some cases, single fMRS voxels could be placed based on the structural scan alone (Table 1). Because fMRS requires prolonged experimental condition and baseline blocks to gain sufficient SNR for low concentration metabolites, identical fMRI runs are needed to justify the fMRS findings. Concomitant fMRI and fMRS scans during functional studies can provide the possibility to justify and interpret modulations of neurochemistry in relation to hemodynamic alterations and help understand underlying excitatory-inhibitory neuromodulation, neuroenergetics and potentially other yet unknown metabolic mechanisms supporting localized functional changes.[49,54–56,93,105] Nevertheless, task-induced changes in tissue metabolite levels cannot be directly related to altered fluxes in energy metabolism and neurotransmitter cycling, which would require multimodal measurements, e.g. ^{1}H-MRS and ^{13}C-MRS or PET.

Conventional fMRI is based on fixed TE observations from the unsuppressed water resonance.

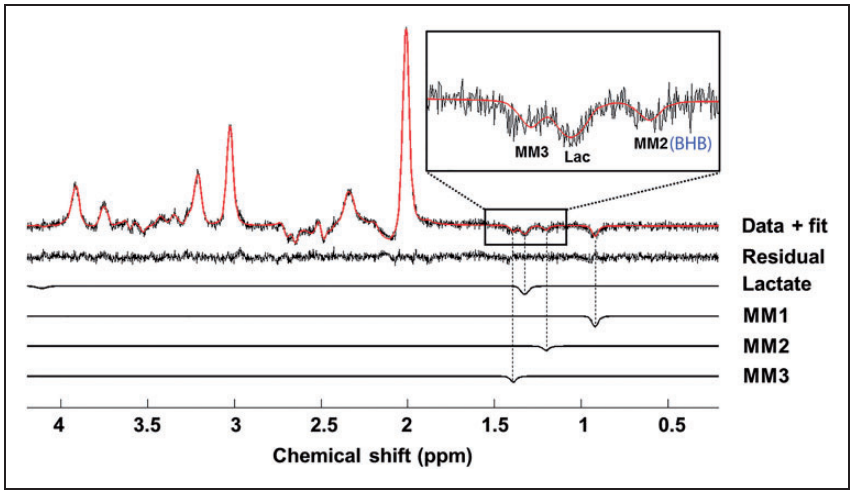

Figure 5. Single subject long TE semi-LASER data and fit for lactate fMRS at 7 T. This data acquisition is similar to editing OFF experiment in lactate JDE MRS acquisitions.[53,54,119] However, in comparison to J-difference spectrum, this method has a lower SNR which may not be sufficient for applications at lower magnetic fields. Macromolecules MM1-MM3 were modelled as Lorentzian peaks,[74] yet as it has been recently shown, the MM2 at 1.20 ppm contains the BHB resonance.[53,54,119] The figure is modified from Fernandez et al.[74]

In contrast, in fMRS acquisitions of metabolites, the water signal, which is several orders of magnitude larger than the metabolites of interest, is suppressed. However, the BOLD response from the single fMRS voxel could be evaluated using the whole free induction decay (FID) of unsuppressed water resonance.[67,68,155,156] Ideally, from an fMRS perspective, the stimulation-induced BOLD response should be evaluated from the same single voxel using the same localization and shimming parameters. This was demonstrated for the first time at 3.0T using a long TE asymmetric PRESS sequence, whereby water was acquired interleaved with water-suppressed metabolite acquisitions (TE = 105 ms, TR = 1500 ms per each water suppressed and unsuppressed acquisition).[84] Thus, assessing water suppressed and unsuppressed fMRS data using the same long TE is feasible. However, it could be suboptimal in terms of the water FID sensitivity to BOLD modulations, because of the reduced FID magnitude and thereby potentially reduced T_2* fitting precision, as compared to the whole FID acquired at short TE.

To concomitantly acquire BOLD-weighted water and J-edited metabolite responses to (de)activation, a diffusion-weighted STEAM sequence for fMRI (TE = 20 ms, mixing time TM = 10 ms, 410 ms delay) was interleaved with MEGA sLASER JDE sequence for GABA and lactate fMRS (TE = 71 ms for GABA, TE = 144 ms for lactate, TR = 2700 ms) (Figure 6(a)).[54] The diffusion weighting (b-value = 1400 s/mm^2, TR = 2700 ms) was applied to reduce intravascular BOLD effects. To provide the functional whole-brain/slab hemodynamic along with metabolite estimates, a conventional fMRI sequence using gradient-echo echo planar imaging (3D EPI; TE = 30 ms, TR = 40 ms, 250 ms delay), was interleaved with fMRS spectra acquisitions using short TE sLASER at 7.0T (TE = 36 ms, TR = 4000 ms) (Figure 6(b)).[55,56] In principle, any fMRI or fMRS techniques could be interleaved given the availability of vendor/custom pulse sequences. Concomitant fMRI-fMRS acquisitions have a temporal shift between fMRI and fMRS acquisitions conditioned by their repetition times and a delay in-between to acquire the FID[54] or to minimize potential eddy current effects from EPI read-out.[56,157]

A potential application of real-time water and J-edited fMRS, as well as interleaved fMRI-fMRS, could be in neurofeedback studies based on BOLD signal. Neurofeedback enables individuals to learn a volitional control of brain circuits implicated in specific behaviors or pathology.[158] Conventional fMRI is based on indirect T_2* mapping at fixed TE. However, tissue T_2* can vary across brain regions and individuals and can be biased by macrovasculature signals at ultra-high magnetic field. Therefore, direct single voxel T_2* estimation based on real-time, short TE PRESS fMRS was proposed to estimate individual (and more physiologically plausible) neurofeedback using the unsuppressed water FID at 3.0T (TE = 30 ms, TR = 1000 ms) and 7.0T (TE = 20 ms, TR = 1000 ms).[67,68,156] Neurofeedback signal was provided to individuals at each repetition time and was based on real-time water spectra preprocessing and T_2*-based feedback estimates. For visual and motor

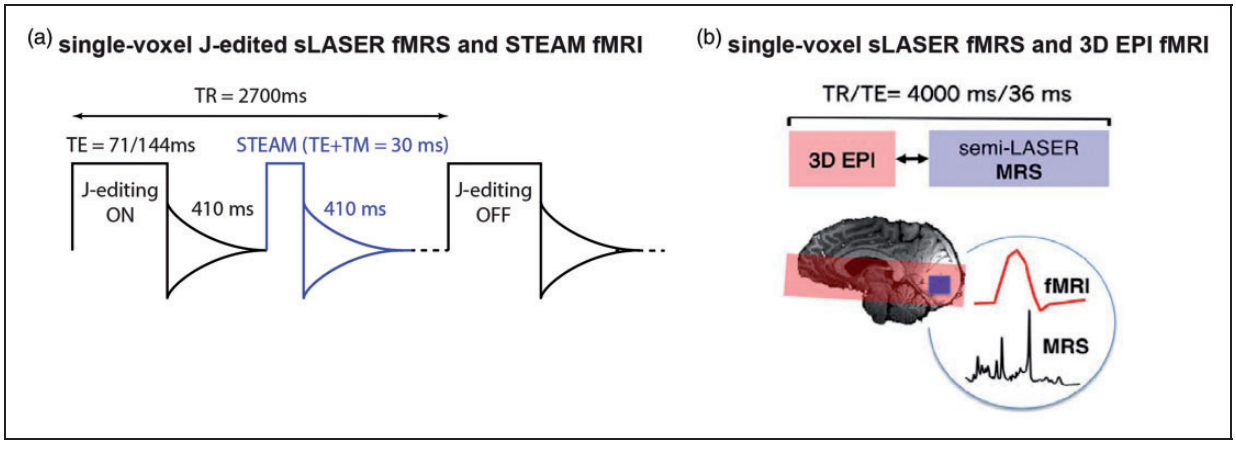

Figure 6. Combined fMRI and fMRS sequences for simultaneous hemodynamic and metabolic observations. (a) To concomitantly acquire single voxel water ^{1}H for BOLD responses and metabolite ^{1}H for metabolic responses, unsuppressed water ^{1}H acquisitions (fMRI) could be interleaved with water-suppressed ^{1}H MEGA-sLASER JDE (fMRS).[54] For fMRS, short TE MRS or JDE MRS for single or multiple metabolites could be used. Water spectra could be acquired using single voxel short TE MRS without water suppression, e.g., using STEAM[163] with diffusion weighting to reduce intravascular BOLD effects (diffusion gradient b = 1400 s/mm^2, 410 ms delay from preceding free induction decay). (b) Partial brain coverage BOLD-fMRI by conventional GE EPI sequence could also be efficiently interleaved with single voxel short TE sLASER ^{1}H MRS.[55,56] Panel (b) is modified from Ip et al.[56]

cortices, BOLD sensitivity of direct T_2* estimates was compared to conventional gradient echo EPI acquisitions at 3.0T and 7.0T[68] and across different T_2* estimation algorithms.[156] The demonstrated feasibility of real-time water fMRS suggests an efficient application of concomitant real-time fMRI-fMRS measurements for neurofeedback research and therapy, benefiting from joint hemodynamic and neurometabolic underpinnings.

Conclusion and future outlook

We reviewed up-to-date fMRS studies, demonstrating that fMRS can be used to investigate metabolic underpinnings of human brain function by measuring metabolic alterations at 3.0T and higher. Non-invasive in vivo assessment of metabolites, like GABA, glutamate, glucose, lactate, glutathione and BHB using fMRS is important for understanding and interpreting brain function in health and disease, providing neurobiological insights into mechanisms underlying excitatory and inhibitory neuromodulation, cerebral blood flow and energy metabolism. Recent fMRS findings demonstrate improved consistency in measurements of basal metabolite levels and their changes, due to progressive improvements of methods benefiting from transition to ultra-high magnetic field and advanced MRI/MRS sequence designs. Short and ultra-short TE spectra acquisitions remain the most common approach for fMRS at 7.0T. Nevertheless, intrinsic elimination of overlapping resonances with JDE MRS and accurate quantification of appropriate metabolites has been shown feasible for fMRS, improving metabolite quantification, especially at the magnetic field below 7.0T (Tables 1 and 2). While MRI at ultra-high magnetic fields improves SNR and has superior tissue contrast, the MRS at ultra-high magnetic field has improved spectral SNR and chemical shift separation, thereby allowing very dilute metabolites to be measured.[57,88,159] Particularly for JDE MRS, ultra-high field increases the ability to resolve overlapping multiplets of J-coupled resonances, contributing to superior spectral quantification. These sensitivity and specificity improvements with ultra-high field allow for smaller physiological and functional effects to be detected. However, acquisitions at ultra-high magnetic field also increases the challenges related to non-uniform RF fields, magnetic susceptibility artifacts, higher RF energy deposition to the tissue, and the requirement for novel magnetic field shimming approaches within spectroscopic voxels.[88]

Due to intrinsic quantum mechanical properties of some target metabolites, JDE MRS at 3.0T has the potential to improve quantitation of fMRS accuracy and replicate metabolic functional changes observed using short TE fMRS at ultra-high field. Recent methodological advances in JDE MRS could be translated to JDE fMRS, such as MR sequence pulse designs for reduction of co-edited lipids/macromolecules,[92,95,96] and advanced editing schemes for quantification of multiple metabolites at 3.0T and 7.0T. When combined with efficient localization approaches, novel JDE schemes could be used in fMRS to segregate multiple metabolites from two voxels simultaneously or from multiple MRSI voxels. JDE fMRS could also extend the number of functionally relevant low concentration metabolites and potentially operate at lower levels of neural (and metabolic) activity.[54] JDE MRS has been shown feasible for highly demanding measurements of glutathione at 3.0T[142,152] and 7.0T,[144] BHB at 4.0T,[53,54] and glucose at 7.0T,[160] emphasizing the potential of JDE fMRS in future studies at 3.0T and 7.0T.

While short-TE MRS is largely considered as the method of choice for 7.0T fMRS, JDE-based MRS can be effectively applied for fMRS at lower magnetic field of 3.0T, thereby substantially increasing the capacity of fMRS methods applied for fundamental and clinical research. Moreover, using 7.0T JDE-based fMRS functional changes in neurotransmitters and neuroenergetics could be observed with significantly improved temporal resolution.[92] We foresee that fMRS observations of functional metabolite alterations will benefit from both low and ultra-high magnetic fields, as well as from both (ultra-)short and JDE MRS methods. To avoid ambiguities regarding effects of habituation from prolonged activations, it is highly recommended to combine fMRS acquisitions with BOLD-based fMRI and even calibrated fMRI[164] for the same paradigm and apply concurrently fMRI-fMRS experiments. Concomitant fMRI-fMRS pulse sequences will provide complementary data for interpretations of hemodynamic and neurochemical alterations associated with excitatory-inhibitory neuromodulation by means of Glu/Gln/GABA levels, and neuroenergetics by means of Glc/Lac levels, both in health and disease. Technological advances of multimodal MRI-PET scanners can further increase the information from neuroimaging.[1,11,24] Finally, real-time water proton fMRS and/or combined fMRI-fMRS acquisitions could be used to provide tissue-specific neurofeedback signal and/or neurofeedback signal accompanied with metabolic observations.

Funding

The author(s) disclosed receipt of the following financial support for the research, authorship, and/or publication of this article: Supported by the National Institutes of Health (R01 NS-100106, R01 MH-067528).

Declaration of conflicting interests

The author(s) declared no potential conflicts of interest with respect to the research, authorship, and/or publication of this article.

ORCID iD

Yury Koush https://orcid.org/0000-0002-3684-5641

References

1. Hyder F and Rothman DL. Advances in imaging brain metabolism. *Annu Rev Biomed Eng* 2017; 19: 485–515. DOI: 10.1146/annurev-bioeng-071516-044450.
2. Hyder F and Rothman DL. Quantitative fMRI and oxidative neuroenergetics. *Neuroimage* 2012; 62: 985–994.
3. Ogawa S, Tank DW, Menon R, et al. Intrinsic signal changes accompanying sensory stimulation: functional brain mapping with magnetic resonance imaging. *Proc Natl Acad Sci U S A* 1992; 89: 5951–5955.
4. Biswal B, Zerrin Yetkin F, Haughton VM, et al. Functional connectivity in the motor cortex of resting human brain using echo-planar MRI. *Magn Reson Med* 1995; 34: 537–541.
5. Buxton RB, Uludağ K, Dubowitz DJ, et al. Modeling the hemodynamic response to brain activation. *Neuroimage* 2004; 23 Suppl 1: S220–233.
6. Ogawa S, Menon RS, Tank DW, et al. Functional brain mapping by blood oxygenation level-dependent contrast magnetic resonance imaging. A comparison of signal characteristics with a biophysical model. *Biophys J* 1993; 64: 803–812.
7. Hoge RD. Calibrated FMRI. *Neuroimage* 2012; 62: 930–937.
8. Tkac I and Gruetter R. Methodology of H NMR spectroscopy of the human brain at very high magnetic fields. *Appl Magn Reson* 2005; 29: 139–157.
9. deGraaf RA. *In vivo NMR spectroscopy*: principles and techniques. Chichester: John Wiley, 2018.
10. Hyder F, Herman P, Bailey CJ, et al. Uniform distributions of glucose oxidation and oxygen extraction in gray matter of normal human brain: No evidence of regional differences of aerobic glycolysis. *J Cereb Blood Flow Metab* 2016; 36: 903–916.
11. Villien M, Wey HY, Mandeville JB, et al. Dynamic functional imaging of brain glucose utilization using fPET-FDG. *Neuroimage* 2014; 100: 192–199.
12. Zheng MQ, Lin SF, Holden D, et al. Comparative evaluation of two glycine transporter 1 radiotracers [11C] GSK931145 and [18F]MK-6577 in baboons. *Synapse* 2016; 70: 112–120.
13. Gunn RN, Murthy V, Catafau AM, et al. Translational characterization of [11C]GSK931145, a PET ligand for the glycine transporter type 1. *Synapse* 2011; 65: 1319–1332.
14. Streffer J, Treyer V, Buck A, et al. Regional brain mGlu5 receptor occupancy following single oral doses of mavoglurant as measured by [(11)C]-ABP688 PET imaging in healthy volunteers. *Neuroimage* 2021; 230: 117785.
15. Sah BR, Sommerauer M, Mu L, et al. Radiation dosimetry of [(18)F]-PSS232-a PET radioligand for imaging mGlu5 receptors in humans. *EJNMMI Res* 2019; 9: 56.
16. Wiebking C, Duncan NW, Qin P, et al. External awareness and GABA–a multimodal imaging study combining fMRI and [18F]flumazenil-PET. *Hum Brain Mapp* 2014; 35: 173–184.
17. Hahn A, Wadsak W, Windischberger C, et al. Differential modulation of the default mode network via serotonin-1A receptors. *Proc Natl Acad Sci U S A* 2012; 109: 2619–2624.
18. Tomasi D, Volkow ND, Wang R, et al. Dopamine transporters in striatum correlate with deactivation in the default mode network during visuospatial attention. *PloS One* 2009; 4: e6102.
19. Chhina N, Kuestermann E, Halliday J, et al. Measurement of human tricarboxylic acid cycle rates during visual activation by (13)C magnetic resonance spectroscopy. *J Neurosci Res* 2001; 66: 737–746.
20. Mangia S, Giove F, Tkac I, et al. Metabolic and hemodynamic events after changes in neuronal activity: current hypotheses, theoretical predictions and in vivo NMR experimental findings. *J Cereb Blood Flow Metab* 2009; 29: 441–463.
21. Mullins PG. Towards a theory of functional magnetic resonance spectroscopy (fMRS): a meta-analysis and discussion of using MRS to measure changes in neurotransmitters in real time. *Scand J Psychol* 2018; 59: 91–103.
22. Mangia S, Giove F and Dinuzzo M. Metabolic pathways and activity-dependent modulation of glutamate concentration in the human brain. *Neurochem Res* 2012; 37: 2554–2561.
23. Stanley JA and Raz N. Functional magnetic resonance spectroscopy: the "new" MRS for cognitive neuroscience and psychiatry research. *Front Psychiatry* 2018; 9: 76.
24. Duncan NW, Wiebking C and Northoff G. Associations of regional GABA and glutamate with intrinsic and extrinsic neural activity in humans-a review of multimodal imaging studies. *Neurosci Biobehav Rev* 2014; 47: 36–52.
25. Siesjo BK. *Brain energy metabolism*. New York: Wiley, 1978.
26. Vaishnavi SN, Vlassenko AG, Rundle MM, et al. Regional aerobic glycolysis in the human brain. *Proc Natl Acad Sci U S A* 2010; 107: 17757–17762.
27. Fox PT and Raichle ME. Focal physiological uncoupling of cerebral blood flow and oxidative metabolism during somatosensory stimulation in human subjects. *Proc Natl Acad Sci U S A* 1986; 83: 1140–1144.
28. Vafaee MS, Vang K, Bergersen LH, et al. Oxygen consumption and blood flow coupling in human motor cortex during intense finger tapping: implication for a role of lactate. *J Cereb Blood Flow Metab* 2012; 32: 1859–1868.
29. Fox PT, Raichle ME, Mintun MA, et al. Nonoxidative glucose consumption during focal physiologic neural activity. *Science* 1988; 241: 462–464.

30. Lin A-L, Fox PT, Hardies J, et al. Nonlinear coupling between cerebral blood flow, oxygen consumption, and ATP production in human visual cortex. *Proc Natl Acad Sci USA* 2010; 107: 8446–8451.
31. Prichard J, Rothman D, Novotny E, et al. Lactate rise detected by 1H NMR in human visual cortex during physiologic stimulation. *Proc Natl Acad Sci U S A* 1991; 88: 5829–5831.
32. Pellerin L and Magistretti PJ. Glutamate uptake into astrocytes stimulates aerobic glycolysis: a mechanism coupling neuronal activity to glucose utilization. *Proc Natl Acad Sci U S A* 1994; 91: 10625–10629.
33. Wyss MT, Jolivet R, Buck A, et al. In vivo evidence for lactate as a neuronal energy source. *J Neurosci* 2011; 31: 7477–7485.
34. Dienel GA. Brain lactate metabolism: the discoveries and the controversies. *J Cereb Blood Flow Metab* 2012; 32: 1107–1138.
35. Bergersen LH and Gjedde A. Is lactate a volume transmitter of metabolic states of the brain? *Front Neuroenergetics* 2012; 4: 5–6.
36. Patel AB, Lai JC, Chowdhury GM, et al. Direct evidence for activity-dependent glucose phosphorylation in neurons with implications for the astrocyte-to-neuron lactate shuttle. *Proc Natl Acad Sci U S A* 2014; 111: 5385–5390.
37. Chen W, Novotny EJ, Zhu XH, et al. Localized 1H NMR measurement of glucose consumption in the human brain during visual stimulation. *Proc Natl Acad Sci U S A* 1993; 90: 9896–9900.
38. Sappey-Marinier D, Calabrese G, Fein G, et al. Effect of photic stimulation on human visual cortex lactate and phosphates using 1H and 31P magnetic resonance spectroscopy. *J Cereb Blood Flow Metab* 1992; 12: 584–592.
39. Frahm J, Kruger G, Merboldt KD, et al. Dynamic uncoupling and recoupling of perfusion and oxidative metabolism during focal brain activation in man. *Magn Reson Med* 1996; 35: 143–148.
40. Merboldt KD, Bruhn H, Hanicke W, et al. Decrease of glucose in the human visual cortex during photic stimulation. *Magn Reson Med* 1992; 25: 187–194.
41. Kuwabara T, Watanabe H, Tsuji S, et al. Lactate rise in the basal ganglia accompanying finger movements: a localized 1H-MRS study. *Brain Res* 1995; 670: 326–328.
42. Urrila AS, Hakkarainen A, Heikkinen S, et al. Metabolic imaging of human cognition: an fMRI/1H-MRS study of brain lactate response to silent word generation. *J Cereb Blood Flow Metab* 2003; 23: 942–948.
43. Urrila AS, Hakkarainen A, Heikkinen S, et al. Stimulus-induced brain lactate: effects of aging and prolonged wakefulness. *J Sleep Res* 2004; 13: 111–119.
44. Hanstock CC, Rothman DL, Prichard JW, et al. Spatially localized 1H NMR spectra of metabolites in the human brain. *Proc Natl Acad Sci U S A* 1988; 85: 1821–1825.
45. Mangia S, Tkac I, Gruetter R, et al. Sustained neuronal activation raises oxidative metabolism to a new steady-state level: evidence from 1H NMR spectroscopy in the human visual cortex. *J Cereb Blood Flow Metab* 2007; 27: 1055–1063.
46. Mangia S, Tkac I, Logothetis NK, et al. Dynamics of lactate concentration and blood oxygen level-dependent effect in the human visual cortex during repeated identical stimuli. *J Neurosci Res* 2007; 85: 3340–3346.
47. Schaller B, Mekle R, Xin L, et al. Net increase of lactate and glutamate concentration in activated human visual cortex detected with magnetic resonance spectroscopy at 7 tesla. *J Neurosci Res* 2013; 91: 1076–1083.
48. Schaller B, Xin L, O'Brien K, et al. Are glutamate and lactate increases ubiquitous to physiological activation? A (1)H functional MR spectroscopy study during motor activation in human brain at 7Tesla. *Neuroimage* 2014; 93: 138–145.
49. Bednařík P, Tkáč I, Giove F, et al. Neurochemical and BOLD responses during neuronal activation measured in the human visual cortex at 7 tesla. *J Cereb Blood Flow Metab* 2015; 35: 601–610.
50. Boillat Y, Xin L, van der Zwaag W, et al. Metabolite concentration changes associated with positive and negative BOLD responses in the human visual cortex: a functional MRS study at 7 tesla. *J Cereb Blood Flow Metab* 2020; 40: 488–500.
51. Giove F, Mangia S, Bianciardi M, et al. The physiology and metabolism of neuronal activation: in vivo studies by NMR and other methods. *Magn Reson Imaging* 2003; 21: 1283–1293.
52. Klingner CM, Hasler C, Brodoehl S, et al. Excitatory and inhibitory mechanisms underlying somatosensory habituation. *Hum Brain Mapp* 2014; 35: 152–160.
53. Koush Y, de Graaf RA, Jiang L, et al. Functional MRS with J-edited lactate in human motor cortex at 4T. *Neuroimage* 2019; 184: 101–108.
54. Koush Y, de Graaf RA, Kupers R, et al. Metabolic underpinnings of activated and deactivated cortical areas in human brain. *J Cereb Blood Flow Metab* 2021; 41: 986–1000.
55. Ip IB, Emir UE, Parker AJ, et al. Comparison of neurochemical and BOLD signal contrast response functions in the human visual cortex. *J Neurosci* 2019; 39: 7968–7975.
56. Ip IB, Berrington A, Hess AT, et al. Combined fMRI-MRS acquires simultaneous glutamate and BOLD-fMRI signals in the human brain. *Neuroimage* 2017; 155: 113–119.
57. Tkac I, Andersen P, Adriany G, et al. In vivo 1H NMR spectroscopy of the human brain at 7 T. *Magn Reson Med* 2001; 46: 451–456.
58. Hetherington HP, Chu WJ, Gonen O, et al. Robust fully automated shimming of the human brain for high-field 1H spectroscopic imaging. *Magn Reson Med* 2006; 56: 26–33.
59. Juchem C, Cudalbu C, Graaf RA, et al. B0 shimming for in vivo magnetic resonance spectroscopy: Experts' consensus recommendations. *NMR Biomed* 2021; 34: e4350.
60. Gruetter R and Tkac I. Field mapping without reference scan using asymmetric echo-planar techniques. *Magn Reson Med* 2000; 43: 319–323.

61. Mlynárik V, Gambarota G, Frenkel H, et al. Localized short-echo-time proton MR spectroscopy with full signal-intensity acquisition. *Magn Reson Med* 2006; 56: 965–970.
62. Mekle R, Mlynárik V, Gambarota G, et al. MR spectroscopy of the human brain with enhanced signal intensity at ultrashort echo times on a clinical platform at 3T and 7T. *Magn Reson Med* 2009; 61: 1279–1285.
63. Bednařík P, Moheet A, Deelchand DK, et al. Feasibility and reproducibility of neurochemical profile quantification in the human hippocampus at 3 T. *NMR Biomed* 2015; 28: 685–693.
64. Terpstra M, Cheong I, Lyu T, et al. Test-retest reproducibility of neurochemical profiles with short-echo, single-voxel MR spectroscopy at 3T and 7T. *Magn Reson Med* 2016; 76: 1083–1091.
65. Volovyk O and Tal A. Increased glutamate concentrations during prolonged motor activation as measured using functional magnetic resonance spectroscopy at 3T. *Neuroimage* 2020; 223: 117338.
66. Zhu XH and Chen W. Observed BOLD effects on cerebral metabolite resonances in human visual cortex during visual stimulation: a functional (1)H MRS study at 4 T. *Magn Reson Med* 2001; 46: 841–847.
67. Koush Y, Elliott MA and Mathiak K. Single voxel proton spectroscopy for neurofeedback at 7 tesla. *Materials* 2011; 4: 1548–1563.
68. Koush Y, Elliott MA, Scharnowski F, et al. Comparison of real-time water proton spectroscopy and echo-planar imaging sensitivity to the BOLD effect at 3 T and at 7 T. *PloS One* 2014; 9: e91620.
69. Bottomley PA. Spatial localization in NMR spectroscopy in vivo. *Ann N Y Acad Sci* 1987; 508: 333–348.
70. Oz G and Tkac I. Short-echo, single-shot, full-intensity proton magnetic resonance spectroscopy for neurochemical profiling at 4 T: validation in the cerebellum and brainstem. *Magn Reson Med* 2011; 65: 901–910.
71. Bednařík P, Tkáč I, Giove F, et al. Neurochemical responses to chromatic and achromatic stimuli in the human visual cortex. *J Cereb Blood Flow Metab* 2018; 38: 347–359.
72. Lin Y, Stephenson MC, Xin L, et al. Investigating the metabolic changes due to visual stimulation using functional proton magnetic resonance spectroscopy at 7T. *J Cereb Blood Flow Metab* 2012; 32: 1484–1495.
73. Mekle R, Kuhn S, Pfeiffer H, et al. Detection of metabolite changes in response to a varying visual stimulation paradigm using short-TE (1) H MRS at 7 T. *NMR Biomed* 2017; 30: e3672.
74. Fernandes CC, Lanz B, Chen C, et al. Measurement of brain lactate during visual stimulation using a long TE semi-LASER sequence at 7 T. *NMR in Biomedicine* 2020; 33: e4223.
75. Taylor R, Neufeld RW, Schaefer B, et al. Functional magnetic resonance spectroscopy of glutamate in schizophrenia and major depressive disorder: anterior cingulate activity during a color-word stroop task. *NPJ Schizophr* 2015; 1: 15028.
76. Taylor R, Schaefer B, Densmore M, et al. Increased glutamate levels observed upon functional activation in the anterior cingulate cortex using the stroop task and functional spectroscopy. *Neuroreport* 2015; 26: 107–112.
77. Kuhn S, Schubert F, Mekle R, et al. Neurotransmitter changes during interference task in anterior cingulate cortex: evidence from fMRI-guided functional MRS at 3 T. *Brain Struct Funct* 2016; 221: 2541–2551.
78. Kolasinski J, Hinson EL, Divanbeighi Zand AP, et al. The dynamics of cortical GABA in human motor learning. *J Physiol* 2019; 597: 271–282.
79. Lally N, Mullins PG, Roberts MV, et al. Glutamatergic correlates of gamma-band oscillatory activity during cognition: a concurrent ER-MRS and EEG study. *Neuroimage* 2014; 85 Pt 2: 823–833.
80. Stanley JA, Burgess A, Khatib D, et al. Functional dynamics of hippocampal glutamate during associative learning assessed with in vivo (1)H functional magnetic resonance spectroscopy. *Neuroimage* 2017; 153: 189–197.
81. Gussew A, Rzanny R, Erdtel M, et al. Time-resolved functional 1H MR spectroscopic detection of glutamate concentration changes in the brain during acute heat pain stimulation. *Neuroimage* 2010; 49: 1895–1902.
82. Gutzeit A, Meier D, Meier ML, et al. Insula-specific responses induced by dental pain. A proton magnetic resonance spectroscopy study. *Eur Radiol* 2011; 21: 807–815.
83. Gutzeit A, Meier D, Froehlich JM, et al. Differential NMR spectroscopy reactions of anterior/posterior and right/left insular subdivisions due to acute dental pain. *Eur Radiol* 2013; 23: 450–460.
84. Apsvalka D, Gadie A, Clemence M, et al. Event-related dynamics of glutamate and BOLD effects measured using functional magnetic resonance spectroscopy (fMRS) at 3T in a repetition suppression paradigm. *Neuroimage* 2015; 118: 292–300.
85. Woodcock EA, Anand C, Khatib D, et al. Working memory modulates glutamate levels in the dorsolateral prefrontal cortex during (1)H fMRS. *Front Psychiatry* 2018; 9: 66.
86. Kupers R, Danielsen ER, Kehlet H, et al. Painful tonic heat stimulation induces GABA accumulation in the prefrontal cortex in man. *Pain* 2009; 142: 89–93.
87. Chiappelli J, Wijtenburg A, Kochunov P, et al. Glutamatergic response to heat pain in schizophrenia. *Schizophrenia Bulletin* 2017; 43: S81–S82.
88. Ladd ME, Bachert P, Meyerspeer M, et al. Pros and cons of ultra-high-field MRI/MRS for human application. *Prog Nucl Magn Reson Spectrosc* 2018; 109: 1–50.
89. Rothman DL, Behar KL, Hetherington HP, et al. Homonuclear 1H double-resonance difference spectroscopy of the rat brain in vivo. *Proc Natl Acad Sci U S A* 1984; 81: 6330–6334.
90. Mescher M, Merkle H, Kirsch J, et al. Simultaneous in vivo spectral editing and water suppression. *NMR Biomed* 1998; 11: 266–272.

91. Baeshen A, Wyss PO, Henning A, et al. Test-Retest reliability of the brain metabolites GABA and glx with JPRESS, PRESS, and MEGA-PRESS MRS sequences in vivo at 3T. *J Magn Reson Imaging* 2020; 51: 1181–1191.
92. Chen C, Sigurdsson HP, Pepes SE, et al. Activation induced changes in GABA: Functional MRS at 7T with MEGA-sLASER. *Neuroimage* 2017; 156: 207–213.
93. Kurcyus K, Annac E, Hanning NM, et al. Opposite dynamics of GABA and glutamate levels in the occipital cortex during visual processing. *J Neurosci* 2018; 38: 9967–9976.
94. Cleve M, Gussew A and Reichenbach JR. In vivo detection of acute pain-induced changes of GABA+ and glx in the human brain by using functional 1H MEGA-PRESS MR spectroscopy. *Neuroimage* 2015; 105: 67–75.
95. Andreychenko A, Boer VO, de Castro CSA, et al. Efficient spectral editing at 7 T: GABA detection with MEGA-sLASER. *Magn Reson Med* 2012; 68: 1018–1025.
96. Edden RA, Puts NA and Barker PB. Macromolecule-suppressed GABA-edited magnetic resonance spectroscopy at 3T. *Magn Reson Med* 2012; 68: 657–661.
97. Floyer-Lea A, Wylezinska M, Kincses T, et al. Rapid modulation of GABA concentration in human sensorimotor cortex during motor learning. *J Neurophysiol* 2006; 95: 1639–1644.
98. Hasler G, van der Veen JW, Grillon C, et al. Effect of acute psychological stress on prefrontal GABA concentration determined by proton magnetic resonance spectroscopy. *Am J Psychiatry* 2010; 167: 1226–1231.
99. Lea-Carnall CA, Williams SR, Sanaei-Nezhad F, et al. GABA modulates Frequency-Dependent plasticity in humans. *iScience* 2020; 23: 101657.
100. Lea-Carnall CA, Trujillo-Barreto NJ, Montemurro MA, et al. Evidence for frequency-dependent cortical plasticity in the human brain. *Proc Natl Acad Sci U S A* 2017; 114: 8871–8876.
101. Michels L, Martin E, Klaver P, et al. Frontal GABA levels change during working memory. *PloS One* 2012; 7: e31933.
102. Hyder F, Patel AB, Gjedde A, et al. Neuronal-glial glucose oxidation and glutamatergic-GABAergic function. *J Cereb Blood Flow Metab* 2006; 26: 865–877.
103. Shulman RG, Rothman DL, Behar KL, et al. Energetic basis of brain activity: implications for neuroimaging. *Trends Neurosci* 2004; 27: 489–495.
104. Rothman DL, Dienel GA, Behar KL, Hyder F, et al. Glucose sparing by glycogenolysis determines the relationship between brain metabolism and neurotransmission. *J Cereb Blood Flow Metab* 2022; (in press)
105. Martinez-Maestro M, Labadie C and Moller HE. Dynamic metabolic changes in human visual cortex in regions with positive and negative blood oxygenation level-dependent response. *J Cereb Blood Flow Metab* 2019; 39: 2295–2307.
106. Patel AB, Rothman DL, Cline GW, et al. Glutamine is the major precursor for GABA synthesis in rat neocortex in vivo following acute GABA-transaminase inhibition. *Brain Res* 2001; 919: 207–220.
107. Bak LK, Schousboe A and Waagepetersen HS. The glutamate/GABA-glutamine cycle: aspects of transport, neurotransmitter homeostasis and ammonia transfer. *J Neurochem* 2006; 98: 641–653.
108. Rothman DL, Behar KL, Hyder F, et al. In vivo NMR studies of the glutamate neurotransmitter flux and neuroenergetics: implications for brain function. *Annu Rev Physiol* 2003; 65: 401–427.
109. McKenna MC, Waagepetersen HS, Schousboe A, et al. Neuronal and astrocytic shuttle mechanisms for cytosolic-mitochondrial transfer of reducing equivalents: current evidence and pharmacological tools. *Biochem Pharmacol* 2006; 71: 399–407.
110. Hawkins RA. The blood-brain barrier and glutamate. *Am J Clin Nutr* 2009; 90: 867S–874S.
111. Kocharyan A, Fernandes P, Tong XK, et al. Specific subtypes of cortical GABA interneurons contribute to the neurovascular coupling response to basal forebrain stimulation. *J Cereb Blood Flow Metab* 2008; 28: 221–231.
112. Bezalel V, Paz R and Tal A. Inhibitory and excitatory mechanisms in the human cingulate-cortex support reinforcement learning: a functional proton magnetic resonance spectroscopy study. *Neuroimage* 2019; 184: 25–35.
113. Maddock RJ, Casazza GA, Fernandez DH, et al. Acute modulation of cortical glutamate and GABA content by physical activity. *J Neurosci* 2016; 36: 2449–2457.
114. Maddock RJ, Casazza GA, Buonocore MH, et al. Vigorous exercise increases brain lactate and glx (glutamate + glutamine): a dynamic 1H-MRS study. *Neuroimage* 2011; 57: 1324–1330.
115. Huang Z, Davis HI, Yue Q, et al. Increase in glutamate/glutamine concentration in the medial prefrontal cortex during mental imagery: a combined functional mrs and fMRI study. *Hum Brain Mapp* 2015; 36: 3204–3212.
116. Newman JC and Verdin E. beta-Hydroxybutyrate: a signaling metabolite. *Annu Rev Nutr* 2017; 37: 51–76.
117. Jiang L, Mason GF, Rothman DL, et al. Cortical substrate oxidation during hyperketonemia in the fasted anesthetized rat in vivo. *J Cereb Blood Flow Metab* 2011; 31: 2313–2323.
118. Chowdhury GM, Jiang L, Rothman DL, et al. The contribution of ketone bodies to basal and activity-dependent neuronal oxidation in vivo. *J Cereb Blood Flow Metab* 2014; 34: 1233–1242.
119. Dacko M and Lange T. Improved detection of lactate and beta-hydroxybutyrate using MEGA-sLASER at 3 T. *NMR in Biomedicine* 2019; : e4100. 32.
120. Muthukumaraswamy SD, Edden RA, Jones DK, et al. Resting GABA concentration predicts peak gamma frequency and fMRI amplitude in response to visual stimulation in humans. *Proceedings of the National Academy of Sciences of the United States of* 2009; 106: 8356–8361.
121. Donahue MJ, Near J, Blicher JU, et al. Baseline GABA concentration and fMRI response. *Neuroimage* 2010; 53: 392–398.
122. Muthukumaraswamy SD, Evans CJ, Edden RA, et al. Individual variability in the shape and amplitude of the BOLD-HRF correlates with endogenous GABAergic inhibition. *Hum Brain Mapp* 2012; 33: 455–465.

123. Jung J, Williams SR, Sanaei Nezhad F, et al. GABA concentrations in the anterior temporal lobe predict human semantic processing. *Sci Rep* 2017; 7: 15748.
124. Stagg CJ, Bachtiar V and Johansen-Berg H. The role of GABA in human motor learning. *Curr Biol* 2011; 21: 480–484.
125. Northoff G, Walter M, Schulte RF, et al. GABA concentrations in the human anterior cingulate cortex predict negative BOLD responses in fMRI. *Nat Neurosci* 2007; 10: 1515–1517.
126. Walter M, Henning A, Grimm S, et al. The relationship between aberrant neuronal activation in the pregenual anterior cingulate, altered glutamatergic metabolism, and anhedonia in major depression. *Arch Gen Psychiatry* 2009; 66: 478–486.
127. Hu Y, Chen X, Gu H, et al. Resting-state glutamate and GABA concentrations predict task-induced deactivation in the default mode network. *J Neurosci* 2013; 33: 18566–18573.
128. Chen X, Fan X, Hu Y, et al. Regional GABA concentrations modulate inter-network resting-state functional connectivity. *Cereb Cortex* 2019; 29: 1607–1618.
129. Levar N, van Leeuwen JMC, Puts NAJ, et al. GABA concentrations in the anterior cingulate cortex are associated with fear network function and fear recovery in humans. *Front Hum Neurosci* 2017; 11: 202.
130. Enzi B, Duncan NW, Kaufmann J, et al. Glutamate modulates resting state activity in the perigenual anterior cingulate cortex - a combined fMRI-MRS study. *Neuroscience* 2012; 227: 102–109.
131. Duncan NW, Enzi B, Wiebking C, et al. Involvement of glutamate in rest-stimulus interaction between perigenual and supragenual anterior cingulate cortex: a combined fMRI-MRS study. *Hum Brain Mapp* 2011; 32: 2172–2182.
132. Falkenberg LE, Westerhausen R, Specht K, et al. Resting-state glutamate level in the anterior cingulate predicts blood-oxygen level-dependent response to cognitive control. *Proc Natl Acad Sci U S A* 2012; 109: 5069–5073.
133. Kapogiannis D, Reiter DA, Willette AA, et al. Posteromedial cortex glutamate and GABA predict intrinsic functional connectivity of the default mode network. *Neuroimage* 2013; 64: 112–119.
134. Arrubla J, Tse DHY, Amkreutz C, et al. GABA concentration in posterior cingulate cortex predicts putamen response during resting state fMRI. *PloS One* 2014; 9: e106609.
135. Bachtiar V, Near J, Johansen-Berg H, et al. Modulation of GABA and resting state functional connectivity by transcranial direct current stimulation. *eLife* 2015; 4: e08789.
136. Stagg CJ, Bachtiar V, Amadi U, et al. Local GABA concentration is related to network-level resting functional connectivity. *eLife* 2014; 3: e01465.
137. Haag L, Quetscher C, Dharmadhikari S, et al. Interrelation of resting state functional connectivity, striatal GABA levels, and cognitive control processes. *Hum Brain Mapp* 2015; 36: 4383–4393.
138. Delli Pizzi S, Chiacchiaretta P, Mantini D, et al. Functional and neurochemical interactions within the amygdala-medial prefrontal cortex circuit and their relevance to emotional processing. *Brain Struct Funct* 2017; 222: 1267–1279.
139. Duncan NW, Wiebking C, Tiret B, et al. Glutamate concentration in the medial prefrontal cortex predicts resting-state cortical-subcortical functional connectivity in humans. *PloS One* 2013; 8: e60312.
140. Schmaal L, Goudriaan AE, van der Meer J, et al. The association between cingulate cortex glutamate concentration and delay discounting is mediated by resting state functional connectivity. *Brain Behav* 2012; 2: 553–562.
141. Bolinger L and Leigh JS. Hadamard spectroscopic imaging (HSI) for multivolume localization. *J Magn Reson* 1988; 80: 162–167.
142. Saleh MG, Oeltzschner G, Chan KL, et al. Simultaneous edited MRS of GABA and glutathione. *Neuroimage* 2016; 142: 576–582.
143. Chan KL, Puts NA, Schar M, et al. HERMES: Hadamard encoding and reconstruction of MEGA-edited spectroscopy. *Magn Reson Med* 2016; 76: 11–19.
144. Saleh MG, Mikkelsen M, Oeltzschner G, et al. Simultaneous editing of GABA and glutathione at 7T using semi-LASER localization. *Magn Reson Med* 2018; 80: 474–479.
145. Oeltzschner G, Saleh MG, Rimbault D, et al. Advanced Hadamard-encoded editing of seven low-concentration brain metabolites: Principles of HERCULES. *Neuroimage* 2019; 185: 181–190.
146. Schulte RF, Lange T, Beck J, et al. Improved two-dimensional J-resolved spectroscopy. *NMR Biomed* 2006; 19: 264–270.
147. Oeltzschner G, Puts NA, Chan KL, et al. Dual-volume excitation and parallel reconstruction for J-difference-edited MR spectroscopy. *Medicine* 2017; 77: 16–22.
148. Pruessmann KP, Weiger M, Scheidegger MB, et al. SENSE: sensitivity encoding for fast MRI. *Magn Reson Med* 1999; 42: 952–962.
149. Chan KL, Oeltzschner G, Schar M, et al. Spatial Hadamard encoding of J-edited spectroscopy using slice-selective editing pulses. *NMR Biomed* 2017; 30: e3688.
150. Boer VO, Klomp DW, Laterra J, et al. Parallel reconstruction in accelerated multivoxel MR spectroscopy. *Magn Reson Med* 2015; 74: 599–606.
151. Bogner W, Gagoski B, Hess AT, et al. 3D GABA imaging with real-time motion correction, shim update and reacquisition of adiabatic spiral MRSI. *Neuroimage* 2014; 103: 290–302.
152. Chan KL, Oeltzschner G, Saleh MG, et al. Simultaneous editing of GABA and GSH with hadamard-encoded MR spectroscopic imaging. *Magn Reson Med* 2019; 82: 21–32.
153. Bogner W, Hangel G, Esmaeili M, et al. 1D-spectral editing and 2D multispectral in vivo(1)H-MRS and (1) H-MRSI – methods and applications. *Anal Biochem* 2017; 529: 48–64.

154. Bogner W, Otazo R and Henning A. Accelerated MR spectroscopic imaging-a review of current and emerging techniques. *NMR Biomed* 2021; 34: e4314.
155. Hennig J, Janz C, Speck O, et al. Functional spectroscopy of brain activation following a single light-pulse – Examinations of the mechanism of the fast initial response. *Int J Imaging Syst Technol* 1995; 6: 203–208.
156. Koush Y, Elliott MA, Scharnowski F, et al. Real-time automated spectral assessment of the BOLD response for neurofeedback at 3 and 7T. *J Neurosci Methods* 2013; 218: 148–160.
157. Hess AT, Tisdall MD, Andronesi OC, et al. Real-time motion and B0 corrected single voxel spectroscopy using volumetric navigators. *Magn Reson Med* 2011; 66: 314–323.
158. Sitaram R, Ros T, Stoeckel L, et al. Closed-loop brain training: the science of neurofeedback. *Nat Rev Neurosci* 2017; 18: 86–100.
159. Yang S, Hu J, Kou Z, et al. Spectral simplification for resolved glutamate and glutamine measurement using a standard STEAM sequence with optimized timing parameters at 3, 4, 4.7, 7, and 9.4T. *Magn Reson Med* 2008; 59: 236–244.
160. Kaiser LG, Hirokazu K, Fukunaga M, et al. Detection of glucose in the human brain with (1) H MRS at 7 tesla. *Magn Reson Med* 2016; 76: 1653–1660.
161. Mullins PG, Rowland LM, Jung RE, et al. A novel technique to study the brain's response to pain: proton magnetic resonance spectroscopy. *Neuroimage* 2005; 26: 642–646.
162. Maddock RJ, Buonocore MH, Lavoie SP, et al. Brain lactate responses during visual stimulation in fasting and hyperglycemic subjects: a proton magnetic resonance spectroscopy study at 1.5 tesla. *Psychiatry Res* 2006; 148: 47–54.
163. Frahm J, Merboldt KD and Hanicke W. Localized proton spectroscopy using stimulated echoes. *J Magn Reson* 1987; 72: 502–508.
164. Chen JJ, Uthayakumar B, Hyder F. Mapping oxidative metabolism in the human brain with calibrated fMRI in health and disease. *J Cereb Blood Flow Metab* 2022. (in press)